Original Article

A signature of five 7-methylguanosine-related genes is a prognostic marker for lung squamous cell carcinoma

Wensheng Liu[1], Ying Wang[2], Paola Ulivi[3], Simona Tavolari[4], Syed A. A. Rizvi[5], Enrico Capobianco[6], Alfons Navarro[7], Yongjun Zhang[8]

[1]Critical Care Medicine Department, Zhejiang Cancer Hospital, Hangzhou, China; [2]Gynecological Oncology Department, Zhejiang Cancer Hospital, Hangzhou, China; [3]Biosciences Laboratory, IRCCS Istituto Romagnolo per lo Studio dei Tumori "Dino Amadori" (IRST), Meldola, Italy; [4]Medical Oncology, IRCCS Azienda Ospedaliero-Universitaria di Bologna, Bologna, Italy; [5]College of Biomedical Sciences, Larkin University, Miami, FL, USA; [6]Department of Computational Science, The Jackson Laboratory, Farmington, CT, USA; [7]Molecular Oncology and Embryology Laboratory, Department of Surgery and Surgical Specializations, Human Anatomy Unit, Faculty of Medicine and Health Sciences, University of Barcelona (UB), Barcelona, Spain; [8]Integration of Traditional Chinese and Western Medicine Department, Zhejiang Cancer Hospital, Hangzhou, China

Contributions: (I) Conception and design: W Liu, Y Zhang; (II) Administrative support: Y Wang; (III) Provision of study materials or patients: Y Wang; (IV) Collection and assembly of data: W Liu; (V) Data analysis and interpretation: Y Zhang; (VI) Manuscript writing: All authors; (VII) Final approval of manuscript: All authors.

Correspondence to: Yongjun Zhang, MM. Integration of Traditional Chinese and Western Medicine Department, Zhejiang Cancer Hospital, 1 Banshan Eastern Road, Hangzhou 310022, China. Email: zhangyj@zjcc.org.cn.

Background: N^7-methylguanosine (m7G) is an important posttranscriptional modification affecting mRNA and tRNA functions and stability. The genes regulating the m7G process have been previously found involved in the carcinogenesis process. We aimed to analyze the role of m7G-related genes as potential prognostic markers for lung squamous cell carcinoma (LSCC).

Methods: Twenty-nine m7G-related genes were selected for the analysis in the LSCC cohort of the Cancer Genome Atlas (TCGA). Univariate, multivariate, and Kaplan-Meier analyses were used to evaluate the predictive value of risk model developed with m7G signature for overall survival (OS). The Gene Ontology (GO) and Kyoto Encyclopedia of Genes and Genomes (KEGG) pathway enrichment analyses of differentially expressed genes (DEGs) were performed for high- and low-risk LSCC groups.

Results: We identified 17 differentially expressed m7G methylation-related genes in LSCC versus normal tissues. The expression of five m7G-related genes (*EIF3D*, *LSM1*, *NCBP2*, *NUDT10*, and *NUDT11*) was identified as an independent prognostic marker for OS in LSCC patients. A risk model with these five m7G-related genes predicted 2-, and 3-year survival rates of 0.623 and 0.626, respectively. The risk score significantly correlated with OS: LSCC patients with a higher risk score had shorter OS ($P<0.01$) and it was associated with lower immune response ($P<0.01$).

Conclusions: We developed a novel m7G-related gene signature that can be of great utility to predict the prognosis for patients with LSCC.

Keywords: Non-small cell lung cancer (NSCLC); N^7-methylguanosine (m7G); The Cancer Genome Atlas (TCGA); prognosis; biomarker

Submitted Sep 26, 2023. Accepted for publication Nov 09, 2023. Published online Nov 27, 2023.
doi: 10.21037/jtd-23-1504
View this article at: https://dx.doi.org/10.21037/jtd-23-1504

Introduction

Lung cancer is one of the most commonly diagnosed cancer and the leading cause of cancer-related deaths in the world, and it continues to be a significant health burden globally (1). Histologically, up to 85% of all lung cancer cases are diagnosed as non-small cell lung cancer (NSCLC), which can be further classified as lung adenocarcinoma (LUAD) or lung squamous cell carcinoma (LSCC) (2). Etiologically, tobacco smoke and various agents that can induce DNA damage and DNA repair deficiency, are the leading risk factors for lung cancer development (3). Tobacco smoke contains thousands of constituents, many of which can damage the genomic DNA and induce normal cell transformation and carcinogenesis (4,5). Clinically, LSCC occurs more frequently in males than in females and is closely associated with tobacco smoke (6). In addition, it is characterized by distinct gene alterations and clinical outcomes compared with those of LUAD (3,7). Advanced LSCC is associated with a very poor patient prognosis due to the lack of early detection biomarkers and treatment options (8,9). Thus, further investigation of NSCLC, including LSCC, could help to elucidate the underlying molecular mechanisms in order to discover novel biomarkers. Especially early detection and prediction of prognosis and treatment outcomes as well as novel strategies for the treatment of this very deadly disease could thus be developed.

The literature indicates, epigenetic alterations, such as RNA methylation, contribute to lung cancer development and progression (10-12). N^7–methylguanosine (m7G) is an endogenous methylated nucleoside found in different RNA molecules; for example, when m7G occurs in RNA messenger (mRNA), it can regulate mRNA export, translation, and splicing (13), and when m7G occurs in RNA transfer (tRNA), it can change tRNA functions to affect mRNA translation and cell growth (14). As is well known, tRNA belongs to a class of noncoding RNAs and serves as a physical link between the amino acids and the ribosomes according to the matched codon in the mRNA molecules (15,16). To date, approximately 90 different modifications that occur in tRNA molecules have been reported (17,18). Although their complete functional implications remain to be determined, m7G is one of the most frequently found in tRNA. If it occurs at position 46 of tRNA, m7G will form a tertiary base pair with C13-G22 to stabilize the 3-dimensional (3D) core of the tRNA (19-21). In addition, m7G modification of tRNA is mediated by the METTL1-WDR4 complex (22), of which METTL1 is a writer of m7G in mRNA and various noncoding RNAs, such as tRNA (23). Gene mutations or altered functions of the enzyme can contribute to human disease; for example, a mutation in the *WDR4* gene will impair tRNA m7G46 methylation and cause microcephalic primordial dwarfism (24,25). Recent studies also have shown that METTL1-mediated m7G editing is important in inhibition of lung cancer cell migration (26,27). Thus, in this study, we assessed the expression of m7G-related genes as a gene signature, which were selected in base of the regulation role of these genes in non-small cell lung cancer (28-30), to predict the prognosis of LSCC patients. We present this article in accordance with the TRIPOD reporting checklist (available at https://jtd.amegroups.com/article/view/10.21037/jtd-23-1504/rc).

Highlight box

Key findings

- We developed a novel N^7-methylguanosine-related gene signature that can be of great utility to predict the prognosis for patients with lung squamous cell carcinoma (LSCC).

What is known and what is new?

- LSCC treatment depends on many factors including the tumor stage, resectability, performance status, and genomic alterations; however, there was not the successfully biomarkers to predict treatment outcomes and prognoses.
- In this study, we identified as an independent prognostic marker for overall survival in LSCC patients.

What is the implication, and what should change now?

- The data from the current study demonstrated that the risk model which we developed in this study could be useful for predicting the prognosis of LSCC patients. We should further promote and validate it.

Methods

Database searching and data downloading

In this study, we first searched the Cancer Genome Atlas (TCGA) database up to November 15, 2022 (https://portal.gdc.cancer.gov) to identify the differentially expressed genes (DEGs) in LSCC samples and downloaded the data of 502 LSCC patients and 49 normal adjacent lung tissues. We then searched the m7G-related genes and the complete clinicopathological information of the patients, including gender, age, tumor-node-metastasis (TNM) stage, tobacco

Table 1 List of 29 m7G-related genes analyzed in this study

Gene	Full name
AGO2	Argonaute RISC catalytic component 2
CYFIP1	Cytoplasmic FMR1 interacting protein 1
DCP2	Decapping mRNA 2
DCPS	Decapping enzyme, scavenger
EIF3D	Eukaryotic translation initiation factor 3 subunit D
EIF4A1	Eukaryotic translation initiation factor 4A1
EIF4E	Eukaryotic translation initiation factor 4E
EIF4E1B	Eukaryotic translation initiation factor 4E family member 1B
EIF4E2	Eukaryotic translation initiation factor 4E family member 2
EIF4E3	Eukaryotic translation initiation factor 4E family member 3
EIF4G3	Eukaryotic translation initiation factor 4 gamma 3
GEMIN5	Gem nuclear organelle associated protein 5
IFIT5	Interferon induced protein with tetratricopeptide repeats 5
LARP1	La ribonucleoprotein 1, translational regulator
LSM1	LSM1 homolog, mRNA degradation-associated
METTL1	Methyltransferase 1, tRNA methylguanosine
NCBP1	Nuclear cap binding protein subunit 1
NCBP2	Nuclear cap binding protein subunit 2
NCBP2L	Nuclear cap binding protein subunit 2 like
NCBP3	Nuclear cap binding protein subunit 3
NSUN2	NOP2/Sun RNA methyltransferase 2
NUDT10	Nudix hydrolase 10
NUDT11	Nudix hydrolase 11
NUDT16	Nudix hydrolase 16
NUDT3	Nudix hydrolase 3
NUDT4	Nudix hydrolase 4
NUDT4B	Nudix hydrolase 4B
SNUPN	Snurportin 1
WDR4	WD repeat domain 4

m7G, N^7-methylguanosine.

smoking history, and survival data. We then included 29 m7G methylation-related genes to construct a risk model for LSCC (*Table 1*) after thoroughly searching the published literature (13) and the Gene Set Enrichment Analysis (GSEA) database (http://www.gsea-msigdb.org/gsea/login.jsp). The study was conducted in accordance with the Declaration of Helsinki (as revised in 2013).

Data analysis

First, the differential expression of all m7G methylation-related genes between LSCC and adjacent normal tissues was determined, and then the data were imported into the limma R package (R Foundation for Statistical Computing, Vienna, Austria), according to a previous study (31). The genes with a log fold change (FC) >0.5 and an adjusted P value <0.001 were defined as DEGs.

Survival analysis and construction of a risk prediction model

First, we associated these 29 m7G methylation-related genes with the survival of LSCC patients using univariate Cox regression survival analysis. Second, we selected genes with a significant P value. The selections were instrumental to construct the risk prediction model by integrating the expression level of each gene and their corresponding coefficients. Third, we defined the risk prediction score as the risk score, and the predictive power of the risk score was used to predict the 1-, 2-, and 3-year survival rates of the patients using receiver operating characteristic (ROC) curve analysis. Finally, we further performed univariate and multivariate Cox regression analyses to identify the most significant independent risk factors for LSCC patients.

Construction of a protein-protein interaction (PPI) network

As the functions of any given gene are mediated through their coding proteins, a PPI network of the 29 m7G methylation-related genes using the igraph package in R was constructed. The PPI network shows the 29 m7G methylation-related genes as nodes, whereas each line connecting two nodes illustrates their biological relationship. Red lines indicate an upregulated correlation, whereas blue lines a downregulated correlation, with the color intensity representing the strength of the correlation.

Gene Ontology (GO) and Kyoto Encyclopedia of Genes and Genomes (KEGG) pathway analyses

Next, we performed GO and KEGG pathway enrichment analyses of the DEGs to identify their interactions and gene

pathways in LSCC development. In brief, based on the risk score (see above), we categorized all patients into a high- or low-risk category using the median risk score as the cut-off value and utilized the limma R package to identify all DEGs between the high- and low-risk categories. Genes were defined as DEGs when the false discovery rate (FDR) <0.05 and $|\log_2 FC| \geq 1$, and then these genes were analyzed for the GO terms and KEGG pathways using the clusterProfiler package in R, according to a previous study (32).

Numeration of the immune infiltration score

The immune response is important in NSCLC, especially in tobacco smoke-related carcinogenesis (33,34). Thus, we profiled the immune cell population and activation of immune-associated pathways in the tumor microenvironment, gene set signatures in different immune cells, and immune-associated pathways from the literature (28) and utilized the molecular signature database to explore their role in LSCC (https://www.gsea-msigdb.org/gsea/msigdb/). The enrichment score of each signature for each LSCC sample was then inferred based on the RNA-sequencing data and the single-sample GSEA (ssGSEA) by using the gene set variation analysis (GSVA) R package.

Statistical analysis

In this study, inlimma R Software package and GraphPad Prism 5.0 (GraphPad Software Inc., La Jolla, CA, USA) were used for statistical analysis. *T*-test was used for comparison among groups difference analysis, ANOVA was used for continuous variables, and categorical variables were analyzed using Chi-square tests. P value less than 0.05 is defined as significance.

Results

Identification of differentially expressed m7G methylation-related genes in LSCC

In this study, the flow chart is shown in *Figure 1*, we first searched the TCGA database for DEGs in 502 LSCC samples versus 49 normal tissue samples and found 17 m7G methylation-related DEGs in LSCC tissues versus normal tissues using the following cut-off values: |logFC| >0.5, FDR <0.05, and P<0.01 (*Figure 2A*). Of these, 14 genes (*NUDT10*, *NUDT3*, *NUDT11*, *SNUPN*, *AGO2*, *WDR4*, *DCPS*, *NCBP1*, *METTL1*, *LSM1*, *NSUN2*, *LARP1*, *NCBP2*, and *EIF3D*) were upregulated in LSCC tissues, whereas 3 genes (*NCBP2L*, *IFIT5*, and *EIF4E3*) were downregulated. We then performed the PPI network analysis and evaluated the relationship among 29 m7G methylation-related genes (*Figure 2B*).

Classification and prognosis prediction of LSCC patients according to the expression of m7G methylation-related genes

We analyzed the consensus clustering of the investigated 29 m7G-related genes in LSCC tissue samples by selecting k=2 to divide these 502 LSCC patients into high- and low-expression clusters (*Figure 3A*). The relationships between the gene expression profile and the clinical features (age ≤60 *vs.* >60 years), TNM stage, history of tobacco smoking, and survival data according to the high- and low-expression clusters) were presented in a heatmap (*Figure 3B*). Although we were unable to find significant differences in the clinical features between these two clusters, we did find a significant difference in the overall survival (OS) of patients between the two clusters (P=0.0062; *Figure 3C*), indicating the usefulness of this gene signature in predicting the prognosis of LSCC patients.

Univariate Cox regression analysis was used for primary screening of the survival-related genes. The results revealed that the expression of five m7G methylation-related genes (*EIF3D*, *LSM1*, *NCBP2*, *NUDT10* and *NUDT11*) was significantly associated with the OS of the LSCC patients (*Figure 4A*). We then performed the least absolute shrinkage and selection operator (LASSO) Cox regression analysis to construct a gene signature using these five genes with the optimum λ value (*Figure 4B*). Subsequently, multivariate Cox regression analysis was performed to calculate the risk score for each LSCC case. The risk model formula for the risk score was as follows: risk score = (–0.005762 × EIF3D exp.) + (–0.007321 × LSM1 exp.) + (–0.005766 × NCBP2 exp.) + (–0.071864 × NUDT10 exp.) + (–0.012726 × NUDT11 exp.). We then classified these patients into high- and low-risk groups based on the cut-off value of the median risk score (*Figure 4C*) and performed principal component analysis (PCA; *Figure 4D*). We found that the LSCC patients with a high-risk score had a significantly shorter OS than those with a low-risk score (P=0.002; *Figure 4E*). Moreover, our ROC analysis revealed that such a risk score was able to predict the 1-, 2-, and 3-year survival rates of LSCC patients after surgery, with area under the curve (AUC) values of 0.542, 0.623, and 0.626, respectively (*Figure 4F*).

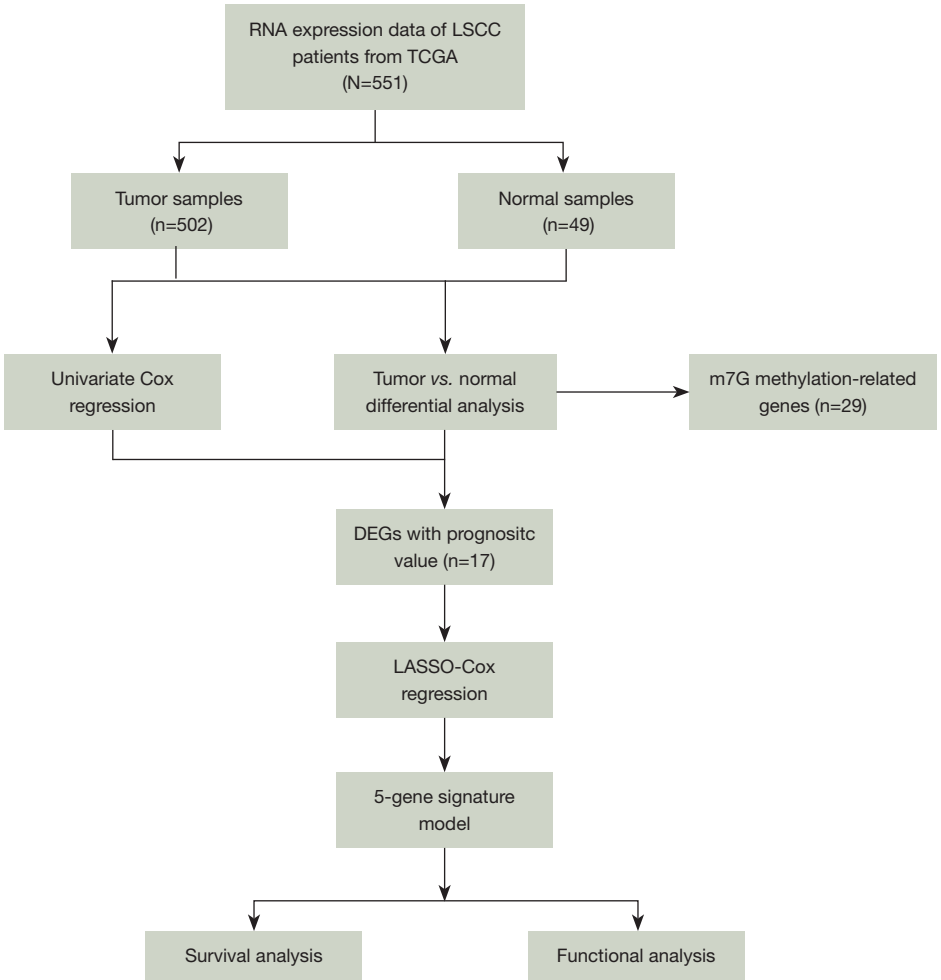

Figure 1 Flow chart of data collection and analysis. LSCC, lung squamous cell carcinoma; TCGA, The Cancer Genome Atlas; m7G, N^7-methylguanosine; DEGs, differentially expressed genes; LASSO, least absolute shrinkage and selection operator.

Identification of the signature of five m7G methylation-related genes as an independent prognostic factor for LSCC patients

Using univariate Cox regression analysis we stated that the higher the risk score was, the worse the prognosis of LSCC [hazard ratio (HR) =1.5503; 95% confidence interval (CI): 1.1585–2.0745; P=0.0032, *Figure 5A*]. To confirm the predictive value of this signature of five m7G methylation-related genes as an independent prognostic factor for LSCC patients, we performed a multivariate Cox regression analyses of the risk score and clinical features of the patients. We found that the risk score was an independent prognostic factor for the LSCC patients, specifically, the higher the risk score was, the worse the prognosis of LSCC (HR =1.57; 95% CI: 1.1702–2.1064; P=0.0026, *Figure 5B*). The pathological stage and the smoking status also emerged as independent factors for OS.

Furthermore, we associated this risk score with the clinicopathological features of the patients and the expression of the individual genes and found that the patients with a high-risk score exhibited significantly lower expression of *NUDT10*, *NUDT11*, *LSM1*, *EIF3D*, and *NCBP2* (*Figure 5C*).

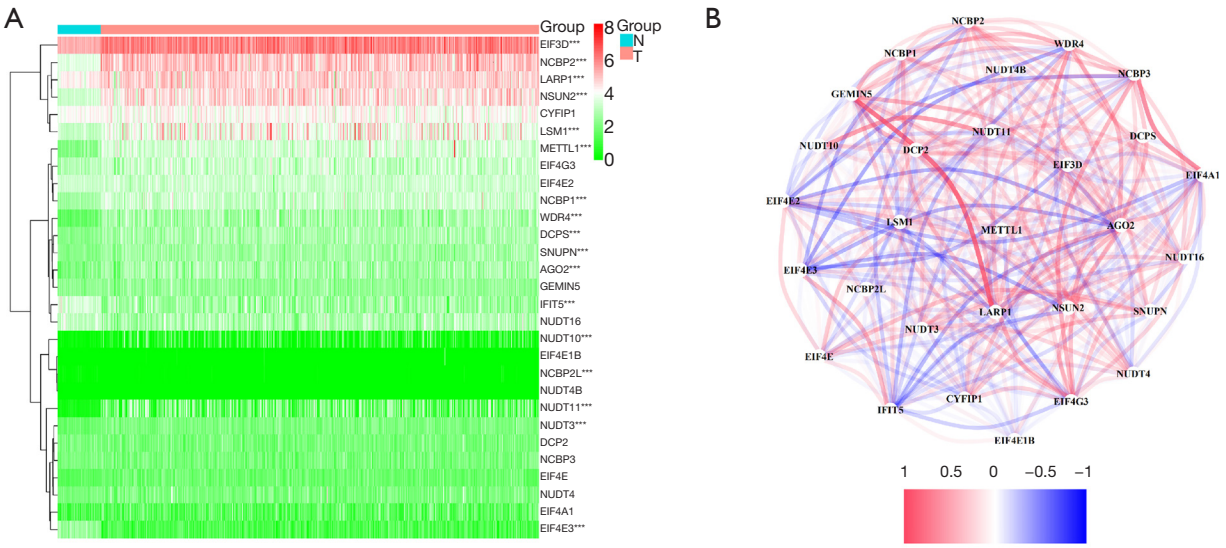

Figure 2 Expression of 29 m7G-related genes in LSCC tissues and their interactions. (A) Heatmap plot showing the expression levels of 29 m7G-related genes in LSCC and normal tissues. The red bars indicate high expression, whereas the green bars refer low expression. (B) PPI network among 29 m7G-related gene-coded proteins. The red bars indicate upregulation, whereas the blue bars refer to downregulation, with the depth of color indicating the strength of the relevance. ***, P<0.001. N, normal tissue; T, tumour tissue; LSCC, lung squamous cell carcinoma; PPI, protein-protein interaction; m7G, N^7-methylguanosine.

Association of the risk score with other biological features of LSCC

According to the risk score, we classified the patients and imported the data into the limma R package to search for the DEGs between the high- and low-risk groups using FDR <0.05 and $|\log_2 FC| \geq 1$. We obtained a total of 496 DEGs (332 upregulated genes and 164 downregulated genes in the high-risk group of patients; Table S1). We then performed GO and KEGG pathway analyses using the clusterProfiler package in R. Our data showed that the DEGs based on the risk model of this signature of five m7G methylation-related genes were mainly correlated with humoral immune response, cellular calcium ion homeostasis, and cytokine-cytokine receptor interaction (*Figure 6A*,*6B*).

Comparison of the immune activity between subgroups

To evaluate the changes in the immune profile according to the risk score of each patient, we enumerated the abundance of different tumor-infiltrating immune cells in the tumor mass using the whole-exome expression data (28) and found that the LSCC patients with high-risk scores had a low immune inflammatory microenvironment, which was shown by significantly lower levels of tumor-infiltrating immune cells such as T- and B-lymphocytes, dendritic cells, macrophages, and neutrophils (*Figure 7A*). After that, we obtained the enrichment scores for 13 immune-associated pathways, such as the cytotoxic activity, antigen presentation, inflammation- promoting, and interferon pathways, to compare their activities between the high- and low-risk cohorts of patients. As shown in *Figure 7B*, the high-risk-scored tumors had significantly lower activations of the pathways related to immune checkpoint activation, cytotoxic activity, antigen presentation, inflammatory response, or type II interferon response.

Discussion

LSCC treatment depends on many factors including the tumor stage, resectability, performance status, and genomic alterations; advanced unresectable LSCC tissues are treated with chemotherapy, radiation therapy, epidermal growth factor receptor (EGFR)-targeted therapy, antiangiogenetic therapy, and/or immune therapy; however, although the decades-long development of vascular endothelial growth factor receptor (VEGFR) inhibition and recent immunotherapy have been shown to improve the survival

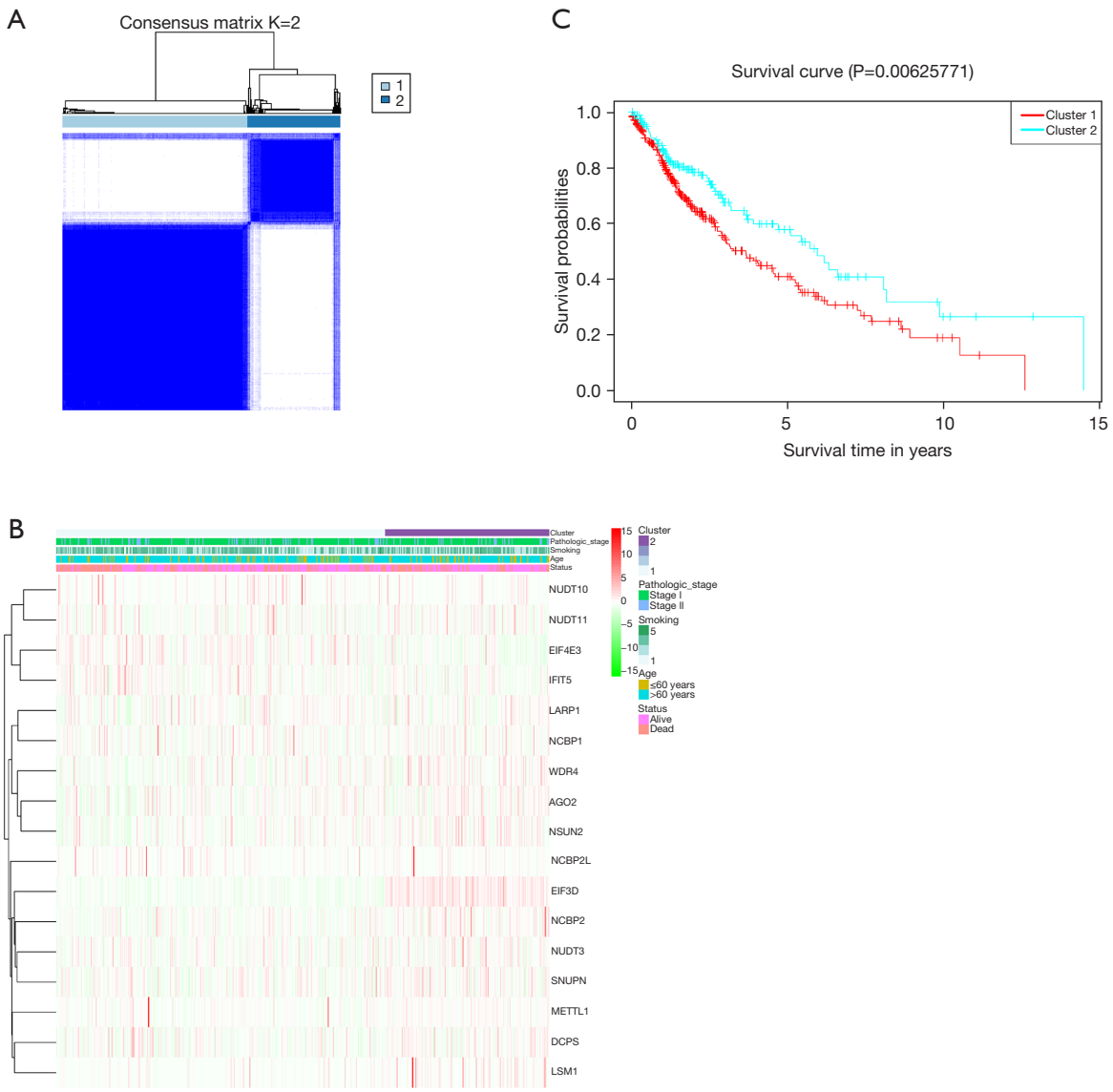

Figure 3 LSCC classification according to the expression level of different m7G-related genes. (A) Illustration of patients according to high and low expression of the m7G-related genes. A total of 502 LSCC patients were divided into high and low expression of the m7G-related genes according to the consensus clustering matrix (k=2). (B) Heat map and the clinicopathological characteristics of the two clusters of different m7G-related gene expression levels. The red bars indicate high expression, whereas the green bars refer low expression. (C) Kaplan-Meier OS curves stratified by the two clusters (P=0.0062). LSCC, lung squamous cell carcinoma; m7G, N^7-methylguanosine; OS, overall survival.

and quality of life of LSCC patients, the effectiveness of LSCC treatment has plateaued for several decades (35,36). At present, predictive biomarkers have been reported in LUAD (37,38), few studies was done in LSCC biomarkers. Thus, it is necessary to search for novel biomarkers could help medical oncologists to successfully predict LSCC treatment outcomes and prognoses. In the current study, we evaluated the prognostic significance of m7G methylation-related gene expression in LSCC tissues and established a signature of five m7G methylation-related genes (*EIF3D*, *LSM1*, *NCBP2*, *NUDT10*, and *NUDT11*) as a risk model to predict the OS of LSCC patients. We found that a high-risk score indicated a worse prognosis for LSCC patients. We also demonstrated that LSCC tissues from patients with

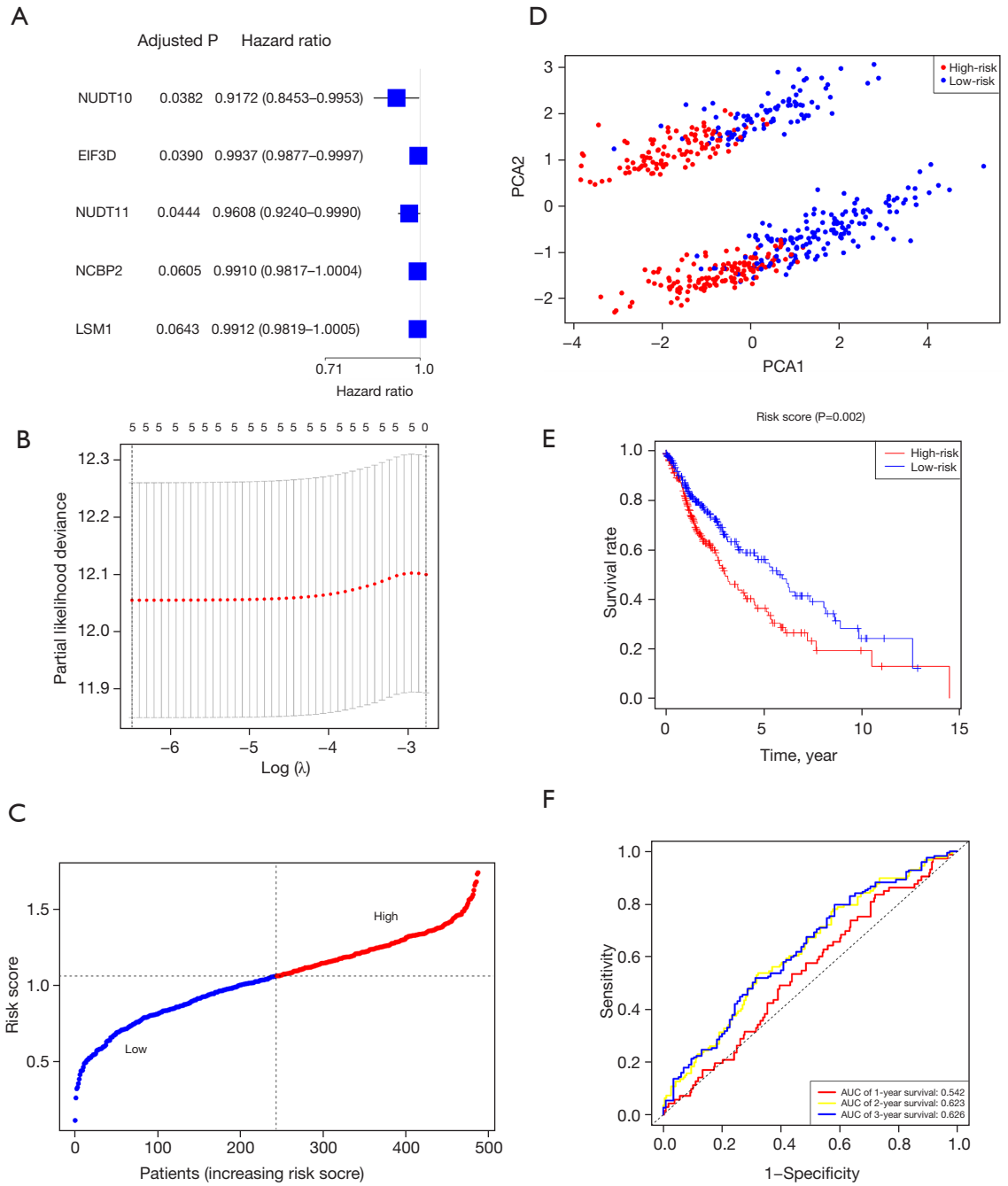

Figure 4 Construction of the risk signature using the TCGA cohort of patients. (A) Univariate Cox regression analysis. The OS of patients with each m7G-related gene and the 5-gene signature was analyzed for their prognostic significance for LSCC patients. (B) The cross-validation using LASSO regression analysis. (C) Identification of the cut-off value of the risk score. LSCC patients were divided into high- or low-risk expression groups using the cut-off value of the median risk score. (D) PCA. Based on the expression levels of the five genes, each patient was accordingly divided into a high- or low-risk group. (E) Kaplan-Meier curves. The survival rates of the LSCC patients were analyzed by using the Kaplan-Meier survival curves and the log rank test stratified by the high- and low-risk scores. (F) ROC curves. The analysis was performed to demonstrate the predictive efficiency of the risk score for LSCC patients. PCA, principal component analysis; AUC, area under the curve; TCGA, The Cancer Genome Atlas; OS, overall survival; m7G, N^7-methylguanosine; LSCC, lung squamous cell carcinoma; LASSO, the least absolute shrinkage and selection operator; ROC, receiver operating characteristic.

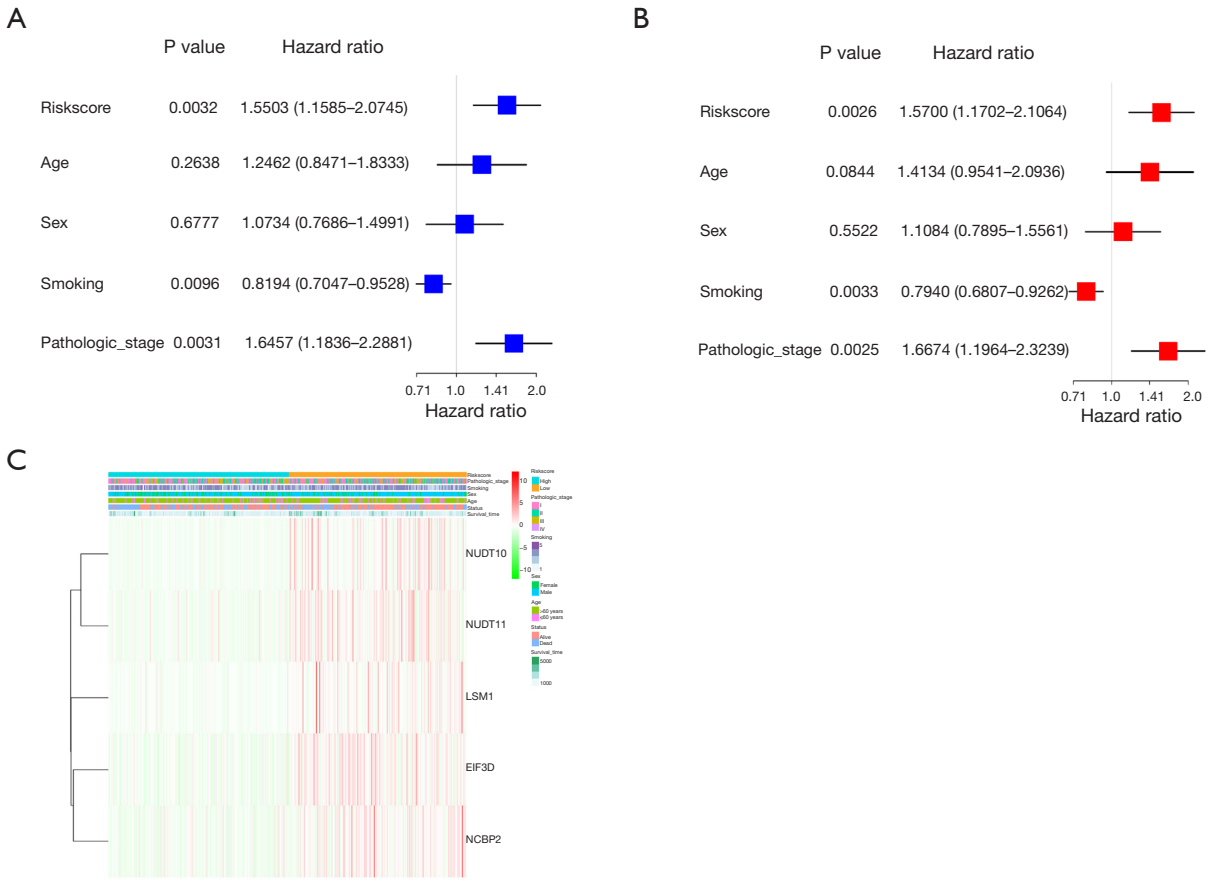

Figure 5 Association of five m7G methylation-related gene signature with the clinicopathological features and prognosis of LSCC patients. (A) Univariate regression analysis. The analysis was performed to associate the prognostic significance of the risk score and other clinicopathological parameters. (B) Multivariate regression analysis. The analysis was used to associate the prognostic significance of the risk score and other clinicopathological parameters. (C) The expression levels of these five genes and their correlation with the risk score and clinicopathological parameters were plotted into the heat map. The red bars indicate high expression, whereas the green bars refer low expression. m7G, N^7-methylguanosine; LSCC, lung squamous cell carcinoma.

a high-risk score were enriched with altered gene pathways that were related to the immune response and inflammatory response.

To the best of our knowledge, this is one of only a few studies of m7G methylation in lung cancer available in the literature (23) that explores the usefulness of m7G methylation-related genes as a predictive marker in LSCC. In the current study, we analyzed 29 m7G methylation-related genes in LSCC tissues versus normal specimens and identified five m7G methylation-related genes as a risk model to estimate the survival of LSCC patients. Specifically, eukaryotic translation initiation factor 3 (EIF3) is necessary for the initiation of protein synthesis in cells and consists of subunits of EIF3A-M; if its subunits are altered, oncogene expression is upregulated, and tumor transformation occurs (39-41). For example, *EIF3D*, as the core subunit of EIF3, plays an oncogenic role in NSCLC (42), and the percentage of apoptotic cells in renal cell carcinoma cells was increased after knockdown of *EIF3D* expression (43). The U6 small nuclear RNA (snRNA)-associated Sm-like protein *LSM1* functions to intimately connect with RNA processing and degradation (44-47). In addition, the downregulation of *LSM1* expression is associated with breast cancer progression (48,49). Moreover, nuclear cap-binding proteins 2 (*NCBP2*) encodes a subunit of the nuclear cap-binding complex to directly contact the 5'-cap through the RNA recognition motif (50) by binding to the 7-methylauanosin cap

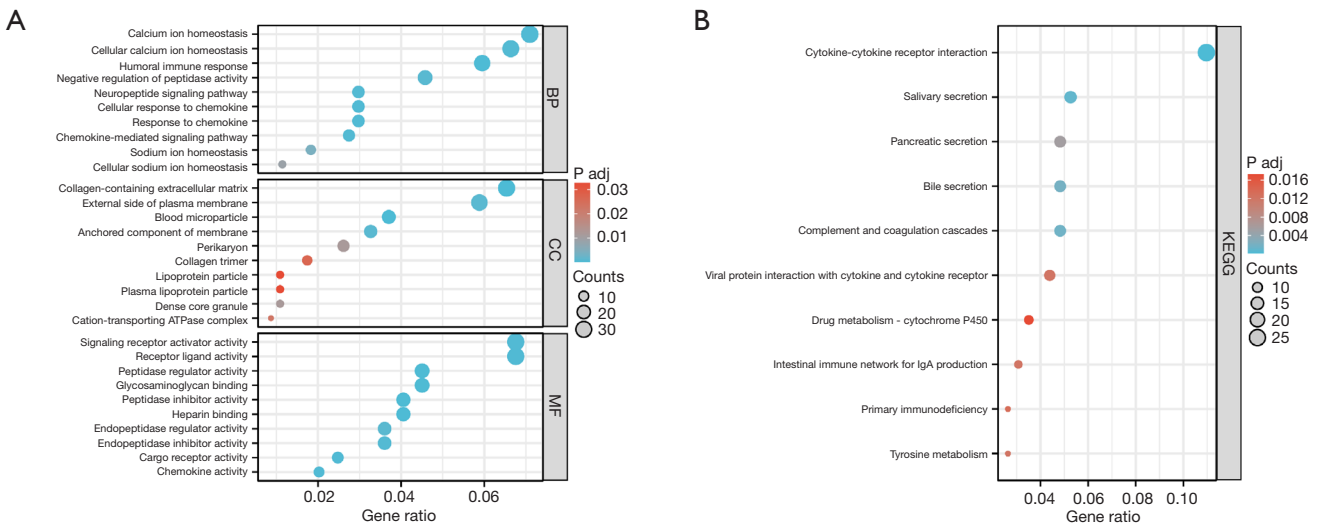

Figure 6 The signature of five m7G methylation-related genes as a prognostic model. (A) Bubble graph of the GO terms. A bigger bubble indicates that more genes are enriched. The increase in the blue color strength indicates a more obvious difference. The q-value is the adjusted P value. (B) Bar plot graph of the KEGG-enriched gene pathways. A longer bar indicates that more genes are enriched. The increase in the blue color intensity indicates that there is a more obvious difference. BP, biological process; CC, cell component; MF, molecular function; m7G, N^7-methylguanosine; KEGG, Kyoto Encyclopedia of Genes and Genomes; GO, Gene Ontology.

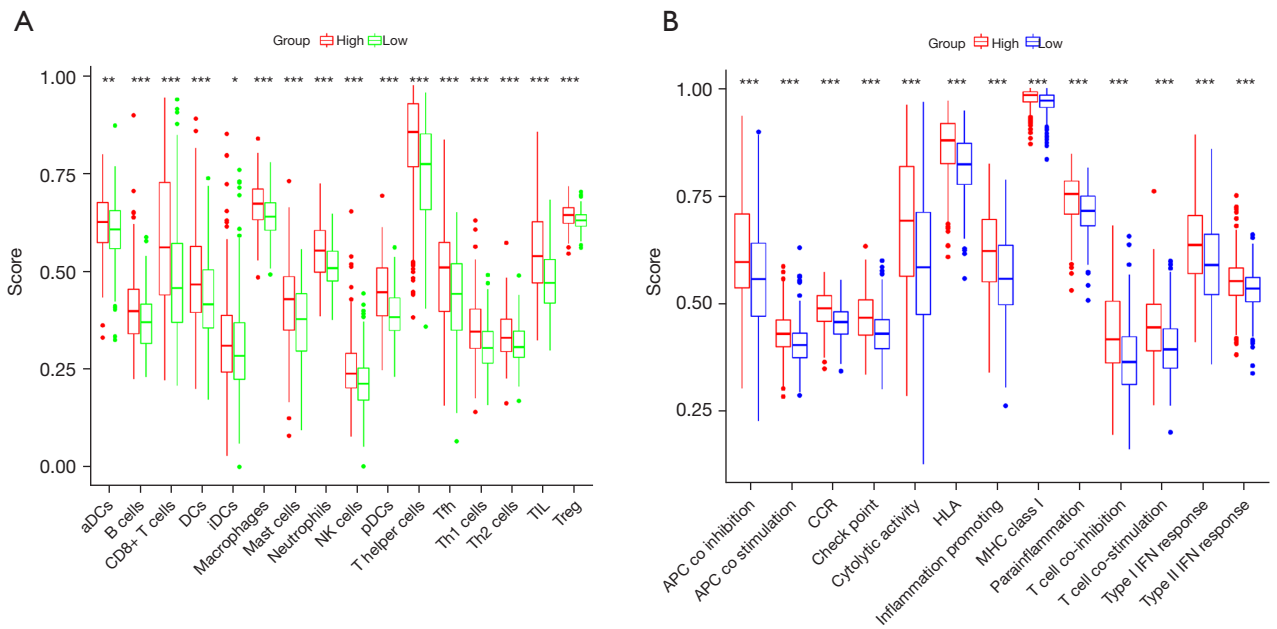

Figure 7 Differential enrichments of 16 immune cell types and 13 immune-related pathways between the high- and low-risk LSCC patients from the TCGA dataset using the signature of five m7G-related genes. The LSCC patients were divided into a high- or low-risk LSCC cohort of the TCGA dataset using the signature of five m7G-related genes, and then the infiltrations of 16 immune cell types and activities of 13 immune-related pathways were compared between these two groups of patients. *, P<0.05; **, P<0.01; ***, P<0.001. aDCs, activated dendritic cell; NK, natural killer; pDCs, plasmacytoid dendritic cell; TIL, tumor infiltrating lymphocyte; APC, Antigen presenting cell; CCR, cytokine-cytokine receptor; HLA, human leukocyte antigen; MHC, major histocompatibility complex; IFN, interferon; LSCC, lung squamous cell carcinoma; TCGA, The Cancer Genome Atlas; m7G, N^7-methylguanosine.

and is then added to the emerging 5'-end of nascent RNA to protect against 5'–3' exonucleolysis (51). A previous study has shown that *NCBP2* can mediate gene interactions to modify neurodevelopmental defects of the 3q29 deletion (52). Additionally, nudix hydroxylases (NUDTs) belong to the versatile, widely distributed, housecleaning enzyme family to catalyze the hydrolysis of a wide range of nucleoside pyrophosphates linked to amino acids (53,54). Furthermore, previous researches have reported that *NUDT10* expression is associated with malignant behaviors of gastric cancer by promoting tumor cell invasion and a poor prognosis (55,56), whereas *NUDT11* has been shown to be associated with longer survival period in liver cancer (57) and bladder cancer (58). In our current study, we revealed that the expression of these five m7G methylation-related genes was associated with a poor prognosis of LSCC patients. However, further investigation is needed to understand their role in LSCC development and progression.

As PPI measurements have increased, more and more PPI network-based protein function prediction methods have been proposed and are generally superior to the homology-based prediction methods (59). We analyzed the PPI among 29 m7G methylation-related genes, and found that *LARP1*, *DCP2* and *GEMIN5* have the strongest positive relevance (the lines among three genes are the reddest). Although the genes regulating the m7G process have been found involved in the carcinogenesis process, the potential modulation between tumor immunity and m7G methylation-related genes remains elusive. Based on the DEGs between different risk groups, we performed GO analyses and discovered that humoral immune responses were enriched. To further explore the correlation between the risk score and immune status, we profiling immune cell populations, immune-associated pathways, and the role of gene set signatures with ssGSEA. Interestingly, we found that the high-risk groups have higher fractions of immune activity. The reason maybe was excessive immune activation promotes immune invasion, and this phenomenon has been found in hepatocellular carcinoma (60,61).

Despite our current data being interesting and potentially useful for determining the prognosis of LSCC patients, this study does have its limitations. For example, we only analyzed the data from the public TCGA database for construction of the risk model for LSCC. The expression of these genes at the protein level needs to be determined to clarify their association with LSCC prognosis. In addition, our current study had no opportunity to validate the expression, functions, and mechanisms of these genes using our own cohort of tissue specimens and cell lines.

Conclusions

The data from the current study demonstrated that detection of the signature of five m7G methylation-related genes could be useful for predicting the prognosis of LSCC patients. Moreover, this five-gene signature is an independent prognostic predictor for the survival of LSCC patients. Our future study will provide validation of our current data using a collection of LSCC samples.

Acknowledgments

Funding: This study was supported in part by a grant from the Zhejiang Provincial Traditional Chinese Medicine Foundation (No. 2019ZA020).

Footnote

Reporting Checklist: The authors have completed the TRIPOD reporting checklist. Available at https://jtd.amegroups.com/article/view/10.21037/jtd-23-1504/rc

Peer Review File: Available at https://jtd.amegroups.com/article/view/10.21037/jtd-23-1504/prf

Conflicts of Interest: All authors have completed the ICMJE uniform disclosure form (available at https://jtd.amegroups.com/article/view/10.21037/jtd-23-1504/coif). The authors have no conflicts of interest to declare.

Ethical Statement: The authors are accountable for all aspects of the work in ensuring that questions related to the accuracy or integrity of any part of the work are appropriately investigated and resolved. The study was conducted in accordance with the Declaration of Helsinki (as revised in 2013).

References

1. Sung H, Ferlay J, Siegel RL, et al. Global Cancer Statistics 2020: GLOBOCAN Estimates of Incidence and Mortality Worldwide for 36 Cancers in 185 Countries. CA Cancer J Clin 2021;71:209-49.
2. Dietel M, Bubendorf L, Dingemans AM, et al. Diagnostic procedures for non-small-cell lung cancer (NSCLC): recommendations of the European Expert Group. Thorax 2016;71:177-84.
3. Balata H, Fong KM, Hendriks LE, et al. Prevention and Early Detection for NSCLC: Advances in Thoracic Oncology 2018. J Thorac Oncol 2019;14:1513-27.
4. Omare MO, Kibet JK, Cherutoi JK, et al. A review of tobacco abuse and its epidemiological consequences. Z Gesundh Wiss 2022;30:1485-500.
5. McRobbie H, Kwan B. Tobacco use disorder and the lungs. Addiction 2021;116:2559-71.
6. Liu B, Liu Y, Zou J, et al. Smoking is Associated with Lung Adenocarcinoma and Lung Squamous Cell Carcinoma Progression through Inducing Distinguishing lncRNA Alterations in Different Genders. Anticancer Agents Med Chem 2022;22:1541-50.
7. Kenfield SA, Wei EK, Stampfer MJ, et al. Comparison of aspects of smoking among the four histological types of lung cancer. Tob Control 2008;17:198-204.
8. Gómez-López S, Whiteman ZE, Janes SM. Mapping lung squamous cell carcinoma pathogenesis through in vitro and in vivo models. Commun Biol 2021;4:937.
9. Pan Y, Han H, Labbe KE, et al. Recent advances in preclinical models for lung squamous cell carcinoma. Oncogene 2021;40:2817-29.
10. Dumitrescu RG. Epigenetic markers of early tumor development. Methods Mol Biol 2012;863:3-14.
11. Brzeziańska E, Dutkowska A, Antczak A. The significance of epigenetic alterations in lung carcinogenesis. Mol Biol Rep 2013;40:309-25.
12. Thapar R, Bacolla A, Oyeniran C, et al. RNA Modifications: Reversal Mechanisms and Cancer. Biochemistry 2019;58:312-29.
13. Zhang LS, Liu C, Ma H, et al. Transcriptome-wide Mapping of Internal N(7)-Methylguanosine Methylome in Mammalian mRNA. Mol Cell 2019;74:1304-1316.e8.
14. Tomikawa C. 7-Methylguanosine Modifications in Transfer RNA (tRNA). Int J Mol Sci 2018;19:4080.
15. Kim SH, Suddath FL, Quigley GJ, et al. Three-dimensional tertiary structure of yeast phenylalanine transfer RNA. Science 1974;185:435-40.
16. Jiao L, Liu Y, Yu XY, et al. Ribosome biogenesis in disease: new players and therapeutic targets. Signal Transduct Target Ther 2023;8:15.
17. Jiapaer Z, Su D, Hua L, et al. Regulation and roles of RNA modifications in aging-related diseases. Aging Cell 2022;21:e13657.
18. Boccaletto P, Stefaniak F, Ray A, et al. MODOMICS: a database of RNA modification pathways. 2021 update. Nucleic Acids Res 2022;50:D231-5.
19. Cui L, Ma R, Cai J, et al. RNA modifications: importance in immune cell biology and related diseases. Signal Transduct Target Ther 2022;7:334.
20. Li J, Zhang H, Wang H. N(1)-methyladenosine modification in cancer biology: Current status and future perspectives. Comput Struct Biotechnol J 2022;20:6578-85.
21. Mattay J. Noncanonical metabolite RNA caps: Classification, quantification, (de)capping, and function. Wiley Interdiscip Rev RNA 2022;13:e1730.
22. Alexandrov A, Martzen MR, Phizicky EM. Two proteins that form a complex are required for 7-methylguanosine modification of yeast tRNA. RNA 2002;8:1253-66.
23. Teng PC, Liang Y, Yarmishyn AA, et al. RNA Modifications and Epigenetics in Modulation of Lung Cancer and Pulmonary Diseases. Int J Mol Sci 2021;22:10592.
24. Shaheen R, Abdel-Salam GM, Guy MP, et al. Mutation in WDR4 impairs tRNA m(7)G46 methylation and causes a distinct form of microcephalic primordial dwarfism. Genome Biol 2015;16:210.
25. Cui W, Zhao D, Jiang J, et al. tRNA Modifications and Modifying Enzymes in Disease, the Potential Therapeutic Targets. Int J Biol Sci 2023;19:1146-62.
26. Pandolfini L, Barbieri I, Bannister AJ, et al. METTL1 Promotes let-7 MicroRNA Processing via m7G Methylation. Mol Cell 2019;74:1278-1290.e9.
27. Chen Y, Xie C, Zheng X, et al. LIN28/let-7/PD-L1 Pathway as a Target for Cancer Immunotherapy. Cancer Immunol Res 2019;7:487-97.
28. Pan J, Huang Z, Lin H, et al. M7G-Related lncRNAs predict prognosis and regulate the immune microenvironment in lung squamous cell carcinoma. BMC Cancer 2022;22:1132.
29. Qiu X, Chen Y, Zhu X, et al. Analysis and Validation of the Prognosis ability of the M7GRelated miRNAs in Lung Adenocarcinoma. Asian Pac J Cancer Prev

2023;24:1275-87.
30. Tao X, Huang R, Xu R, et al. A novel m7G methylation-related signature associated with chromosome homeostasis in patients with lung adenocarcinoma. Front Genet 2022;13:998258.
31. Liu S, Wang Z, Zhu R, et al. Three Differential Expression Analysis Methods for RNA Sequencing: limma, EdgeR, DESeq2. J Vis Exp 2021.
32. Yu G, Wang LG, Han Y, et al. clusterProfiler: an R package for comparing biological themes among gene clusters. OMICS 2012;16:284-7.
33. Yuan H, Liu J, Zhang J. The Current Landscape of Immune Checkpoint Blockade in Metastatic Lung Squamous Cell Carcinoma. Molecules 2021;26:1392.
34. Hendry S, Salgado R, Gevaert T, et al. Assessing Tumor-Infiltrating Lymphocytes in Solid Tumors: A Practical Review for Pathologists and Proposal for a Standardized Method from the International Immuno-Oncology Biomarkers Working Group: Part 2: TILs in Melanoma, Gastrointestinal Tract Carcinomas, Non-Small Cell Lung Carcinoma and Mesothelioma, Endometrial and Ovarian Carcinomas, Squamous Cell Carcinoma of the Head and Neck, Genitourinary Carcinomas, and Primary Brain Tumors. Adv Anat Pathol 2017;24:311-35.
35. Sasa GBK, Xuan C, Chen M, et al. Clinicopathological implications of lncRNAs, immunotherapy and DNA methylation in lung squamous cell carcinoma: a narrative review. Transl Cancer Res 2021;10:5406-29.
36. Tian Y, Zhai X, Yan W, et al. Clinical outcomes of immune checkpoint blockades and the underlying immune escape mechanisms in squamous and adenocarcinoma NSCLC. Cancer Med 2021;10:3-14.
37. Tran TO, Vo TH, Lam LHT, et al. ALDH2 as a potential stem cell-related biomarker in lung adenocarcinoma: Comprehensive multi-omics analysis. Comput Struct Biotechnol J 2023;21:1921-9.
38. Dang HH, Ta HDK, Nguyen TTT, et al. Prospective role and immunotherapeutic targets of sideroflexin protein family in lung adenocarcinoma: evidence from bioinformatics validation. Funct Integr Genomics 2022;22:1057-72.
39. Yi SH, Petrychenko V, Schliep JE, et al. Conformational rearrangements upon start codon recognition in human 48S translation initiation complex. Nucleic Acids Res 2022;50:5282-98.
40. Ma S, Liu JY, Zhang JT. eIF3d: A driver of noncanonical cap-dependent translation of specific mRNAs and a trigger of biological/pathological processes. J Biol Chem 2023;299:104658.
41. Rubio A, Garland GD, Sfakianos A, et al. Aberrant protein synthesis and cancer development: The role of canonical eukaryotic initiation, elongation and termination factors in tumorigenesis. Semin Cancer Biol 2022;86:151-65.
42. Wang D, Jia Y, Zheng W, et al. Overexpression of eIF3D in Lung Adenocarcinoma Is a New Independent Prognostic Marker of Poor Survival. Dis Markers 2019;2019:6019637.
43. Chen M, Nie Z, Gao Y, et al. m7G regulator-mediated molecular subtypes and tumor microenvironment in kidney renal clear cell carcinoma. Front Pharmacol 2022;13:900006.
44. Kok Kilic G, Isik E, Alpay O, et al. LSM1 is the new candidate gene for neurodevelopmental disorder. Eur J Med Genet 2022;65:104610.
45. Zhu J, Chen K, Sun YH, et al. LSM1-mediated Major Satellite RNA decay is required for nonequilibrium histone H3.3 incorporation into parental pronuclei. Nat Commun 2023;14:957.
46. He F, Jacobson A. Eukaryotic mRNA decapping factors: molecular mechanisms and activity. FEBS J 2023;290:5057-85.
47. Voutsadakis IA. Characteristics and Prognosis of 8p11.23-Amplified Squamous Lung Carcinomas. J Clin Med 2023;12:1711.
48. Tzeng YT, Tsui KH, Tseng LM, et al. Integrated analysis of pivotal biomarker of LSM1, immune cell infiltration and therapeutic drugs in breast cancer. J Cell Mol Med 2022;26:4007-20.
49. Voutsadakis IA. 8p11.23 Amplification in Breast Cancer: Molecular Characteristics, Prognosis and Targeted Therapy. J Clin Med 2020;9:3079.
50. Calero G, Wilson KF, Ly T, et al. Structural basis of m7GpppG binding to the nuclear cap-binding protein complex. Nat Struct Biol 2002;9:912-7.
51. Pabis M, Neufeld N, Shav-Tal Y, et al. Binding properties and dynamic localization of an alternative isoform of the cap-binding complex subunit CBP20. Nucleus 2010;1:412-21.
52. Singh MD, Jensen M, Lasser M, et al. NCBP2 modulates neurodevelopmental defects of the 3q29 deletion in Drosophila and Xenopus laevis models. PLoS Genet 2020;16:e1008590.
53. Gong J, Yang J, He Y, et al. Construction of m7G subtype classification on heterogeneity of sepsis. Front Genet 2022;13:1021770.
54. Malik A, Hept MA, Purcell EB. Sound the (Smaller)

Alarm: The Triphosphate Magic Spot Nucleotide pGpp. Infect Immun 2023;91:e0043222.
55. Li XY, Wang SL, Chen DH, et al. Construction and Validation of a m7G-Related Gene-Based Prognostic Model for Gastric Cancer. Front Oncol 2022;12:861412.
56. Chen D, Zhang R, Xie A, et al. Clinical correlations and prognostic value of Nudix hydroxylase 10 in patients with gastric cancer. Bioengineered 2021;12:9779-89.
57. Ren S, Cao W, Ma J, et al. Correlation evaluation between cancer microenvironment related genes and prognosis based on intelligent medical internet of things. Front Genet 2023;14:1132242.
58. Li DX, Feng DC, Wang XM, et al. M7G-related molecular subtypes can predict the prognosis and correlate with immunotherapy and chemotherapy responses in bladder cancer patients. Eur J Med Res 2023;28:55.
59. Wu Z, Liao Q, Liu B. A comprehensive review and evaluation of computational methods for identifying protein complexes from protein-protein interaction networks. Brief Bioinform 2020;21:1531-48.
60. Zhang Q, He Y, Luo N, et al. Landscape and Dynamics of Single Immune Cells in Hepatocellular Carcinoma. Cell 2019;179:829-845.e20.
61. Zhou SL, Zhou ZJ, Hu ZQ, et al. Tumor-Associated Neutrophils Recruit Macrophages and T-Regulatory Cells to Promote Progression of Hepatocellular Carcinoma and Resistance to Sorafenib. Gastroenterology 2016;150:1646-1658.e17.

Cite this article as: Liu W, Wang Y, Ulivi P, Tavolari S, Rizvi SAA, Capobianco E, Navarro A, Zhang Y. A signature of five 7-methylguanosine-related genes is a prognostic marker for lung squamous cell carcinoma. J Thorac Dis 2023;15(11):6265-6278. doi: 10.21037/jtd-23-1504

Table S1 The DEGs between the high- and low-risk groups

Gene	Group1mea	Group2mea	LogFC	P	FDR
GSTA1	119.30957	53.407518	-1.159595	2.22E-07	1.98E-06
CADM3	0.5114032	1.110377	1.1185164	0.0001441	0.0005107
WSCD2	1.0979913	0.4998583	-1.135275	9.20E-06	4.80E-05
STK32A	0.2989113	0.6327758	1.0819768	0.002828	0.006716
CIDEC	0.0201461	0.1187589	2.5594629	0.0006198	0.0018094
CSF3	1.3249028	2.7058229	1.0301809	2.47E-05	0.0001123
CCL23	0.4834595	1.0264201	1.0861543	4.08E-07	3.31E-06
TNFSF8	0.6018465	1.6831362	1.4836845	1.21E-08	1.73E-07
ORM1	1.4788369	4.0196725	1.442615	0.0005261	0.0015686
FRMPD2	0.0289142	0.0618396	1.0967539	0.028764	0.0495973
IL13	0.0160907	0.0348177	1.1135932	4.26E-05	0.0001781
AGT	1.0566248	2.3984332	1.182629	0.0006545	0.0018913
PGC	5.287444	14.261942	1.4315281	0.0066703	0.0140788
TEX15	0.1639878	0.0770998	-1.088789	0.0008372	0.0023361
C20orf141	0.0345975	0.1393559	2.0100354	0.0008345	0.0023298
ACOD1	0.0360843	0.0855847	1.2459829	5.26E-06	2.96E-05
MSLN	10.286876	31.556362	1.617126	0.0004684	0.001422
SERPINC1	0.0601158	0.2965276	2.3023501	0.0111534	0.0219257
VNN1	1.5499033	3.8359364	1.3074006	1.34E-07	1.30E-06
GABRA5	0.9388006	0.2926749	-1.68152	2.71E-07	2.34E-06
P2RY8	1.0799028	2.210959	1.0337708	8.89E-10	2.05E-08
IFNL1	0.0974198	0.2025459	1.0559621	0.0147453	0.0279398
PPP1R1A	0.1384413	0.3480803	1.3301457	0.021122	0.038149
CST2	1.4196533	2.9289181	1.0448292	0.0260699	0.045686
ALDH8A1	2.0988422	0.2895775	-2.857572	9.24E-05	0.0003466
ADAMTSL4	2.0347758	4.4272102	1.121528	1.33E-12	1.21E-10
PAX5	0.3757392	0.8873543	1.2397788	0.0039217	0.0088838
GPR39	0.5440864	1.0894654	1.0017126	6.65E-10	1.62E-08
ADGRG5	0.4696084	1.0033527	1.0952989	5.37E-11	2.22E-09
SP7	0.1006116	0.0367602	-1.452579	0.0276112	0.0478971
CLDN17	0.5229669	0.1199531	-2.12425	0.0008374	0.0023361
PLA2G2A	1.7828705	20.097408	3.4947356	0.0005887	0.0017327
CNTNAP5	0.1243809	0.0501248	-1.311169	7.48E-08	7.87E-07
CT55	0.2924818	0.1155466	-1.339872	0.0173173	0.0322273
CD22	0.8764953	2.231673	1.3483073	6.56E-06	3.59E-05
PIANP	1.1661974	0.4536655	-1.362111	4.51E-06	2.58E-05
MPPED1	1.5738907	0.4974811	-1.661622	1.64E-12	1.37E-10
SOHLH1	5.6706693	2.757831	-1.039985	2.42E-06	1.52E-05
SCN3A	0.0755368	0.4372819	2.5333125	0.0054617	0.0118135
DRD2	0.6202069	0.2474827	-1.325422	0.0128504	0.0247754
VTN	0.1736664	6.2286499	5.1645288	1.88E-05	8.88E-05
DBH	0.1497589	0.3542038	1.2419376	6.72E-08	7.21E-07
FCN3	2.030187	5.2274859	1.3645046	2.56E-08	3.20E-07
SERPIND1	1.0064797	2.107477	1.0661988	0.0102982	0.020451
PAX3	0.3297332	0.1299508	-1.343333	3.04E-09	5.51E-08
CCKBR	0.5454668	0.1943434	-1.488883	0.0007384	0.0020985
STEAP4	2.0782922	4.6456707	1.1604884	4.11E-05	0.0001728
CPN2	0.0288832	0.0593193	1.0382728	0.0113382	0.022238
PCP4	0.9534578	5.5791387	2.5488015	0.0006471	0.0018737
GOLT1A	1.4891756	3.5540095	1.2549336	6.02E-05	0.000239
ATP1A4	0.0147874	0.0604297	2.0308896	3.21E-09	5.75E-08
MAP1LC3C	0.2243277	0.5450135	1.2806841	1.52E-08	2.09E-07
NPTX1	0.5228219	2.2119027	2.0808965	0.0180774	0.033396
MROH2B	0.0032195	0.0091915	1.51347	0.0007627	0.0021561
CA4	0.2843025	0.6227929	1.1313259	0.0018923	0.0047507
NPSR1	1.339885	0.3883474	-1.786689	5.89E-08	6.46E-07
SEMA6D	3.934652	1.7872838	-1.138467	3.06E-10	8.67E-09
FCN2	0.0295632	0.0693072	1.2292006	6.24E-06	3.45E-05
INSM1	1.0240897	2.50897	1.2927531	0.027377	0.0475647
NUGGC	0.3880954	0.8082881	1.0584584	1.16E-08	1.67E-07
GSC2	0.105171	0.0302553	-1.797478	1.34E-05	6.66E-05
GRID2	0.0313828	0.0112142	-1.484641	0.000625	0.0018231
CTAG2	9.2477952	3.4118323	-1.438563	0.0160524	0.0301461
SORCS3	0.1587759	0.0743521	-1.094546	0.0020648	0.0051278
CCL25	0.1470561	0.4807973	1.7090625	0.0060054	0.0128516
MUCL3	0.0940217	0.2219138	1.238934	0.0008972	0.0024794
RGL3	0.8105624	1.6804438	1.0518471	1.03E-08	1.51E-07
SCG5	2.0525708	4.4616272	1.120138	0.0274333	0.0476438
EMILIN3	2.9174184	1.123392	-1.376831	1.09E-10	3.79E-09
ADH1C	45.639977	10.232949	-2.157076	0.0256877	0.0451052
SLC17A3	0.0060179	0.0129816	1.1091307	0.0089736	0.0181639
RETN	0.7017673	1.4824505	1.0789192	2.71E-05	0.0001216
XKR4	0.044557	0.1182649	1.4082975	0.0038909	0.0088309
MLPH	2.5026448	5.2133661	1.0587616	1.90E-09	3.79E-08
CAPN8	0.8835729	2.258471	1.3539254	1.15E-06	7.98E-06
AQP4	3.3079876	7.2956026	1.1410733	0.004581	0.0101492
ADCY2	0.5535574	0.2255663	-1.295181	9.90E-07	7.02E-06
SLC5A11	0.28141	0.119367	-1.237269	0.0054716	0.0118334
LRRTM4	0.2675385	0.0692394	-1.950081	4.87E-05	0.000199
CCL14	0.1344315	0.2876892	1.0976397	2.27E-05	0.0001047
PAX1	0.3951162	0.155655	-1.343925	0.0005598	0.0016579
IL5RA	0.1196455	0.2549315	1.0913434	2.27E-05	0.0001048
GPR149	0.6518866	0.2182985	-1.578319	6.25E-05	0.0002466
IL1RL1	0.3603949	1.6073213	2.157008	6.37E-05	0.0002506
ANXA13	0.0948724	0.7648273	3.0110733	0.0003347	0.0010592
BHMT2	0.3884797	1.237061	1.6710054	4.15E-08	4.82E-07
KCNV1	0.1084423	0.0537609	-1.012298	0.0036036	0.0082726
AOC1	1.0058303	2.1078967	1.0674172	6.15E-07	4.70E-06
NTSR1	0.2856177	0.5997247	1.0702152	0.0092096	0.0185709
CCDC38	0.1348066	0.0470407	-1.518909	6.83E-08	7.28E-07
CYP21A2	0.0440292	0.0944784	1.1015237	0.0001009	0.0003747
SELE	1.0779568	2.1753604	1.0129551	0.0001475	0.0005207
S100A7	95.997287	304.17124	1.6638182	0.0026976	0.0064402
ZBTB16	0.1483667	0.3550944	1.2590352	2.82E-06	1.73E-05
ORM2	0.6491734	2.6314422	2.0191778	3.08E-05	0.0001352
BRS3	0.0234084	0.0104029	-1.170035	0.0002266	0.000755
GPIHBP1	0.5306399	1.090285	1.0389003	0.0003318	0.0010513
NR0B2	0.1567234	1.5188267	3.2766649	8.18E-05	0.0003113
HRASLS	5.4470309	2.6297247	-1.050558	5.06E-12	3.35E-10
SLC6A17	0.1629988	0.3365413	1.0459223	0.0001811	0.0006212
NR4A3	1.0782567	2.3099094	1.0991355	0.0006408	0.0018609
ITIH5	0.6259142	1.3904584	1.1515238	0.0001234	0.0004459
HNF1B	0.1838927	0.5626309	1.6133249	3.36E-06	2.01E-05
LINGO4	0.0245577	0.0617063	1.3292417	1.63E-05	7.88E-05
DIO1	0.0867225	0.2442391	1.4938166	1.93E-05	9.08E-05
UBXN10	0.615664	1.3361742	1.117893	1.72E-07	1.59E-06
IL26	0.0473022	0.0996557	1.0750458	6.97E-09	1.10E-07
LAIR2	0.2628627	0.5292187	1.0095548	1.90E-09	3.78E-08
FOSB	7.4376511	17.942147	1.2704336	1.32E-05	6.55E-05
OTX2	0.7495933	0.3498659	-1.099306	2.31E-05	0.0001063
OTOG	0.0485864	0.0210895	-1.204029	0.0004104	0.0012656
SPINK1	1.1273931	9.005926	2.997884	0.0008288	0.0023181
NLRP7	0.4461963	1.0882159	1.2862142	3.31E-07	2.77E-06
MS4A1	1.3341422	3.7868473	1.5050848	0.0005229	0.0015609
NPY4R	0.0317115	0.0731085	1.2050309	5.77E-08	6.35E-07
GKN2	0.3856659	1.0333298	1.4218772	0.0001663	0.0005773
ATRNL1	0.6588255	0.3018433	-1.126097	5.54E-08	6.14E-07
S100A7A	1.7840619	4.7492349	1.4125294	0.0047102	0.0103972
SFTPD	28.733238	63.010375	1.1328688	3.63E-05	0.000156
PLN	1.8326553	4.0171271	1.1322287	3.27E-07	2.75E-06
SLC25A48	0.3206197	0.1464824	-1.130135	5.86E-06	3.26E-05
FCRL2	0.3314166	0.9555507	1.5276868	1.42E-06	9.65E-06
CXCL2	7.9372941	15.968867	1.0085427	1.14E-08	1.65E-07
ASCL4	0.6322416	0.1856614	-1.767802	2.87E-05	0.0001275
SYT9	0.3172504	0.1187185	-1.418077	4.51E-05	0.0001868
CALHM1	0.0482048	0.1009234	1.0660129	0.0153393	0.0289444
VAX1	0.3424188	0.1543036	-1.149991	1.31E-07	1.27E-06
MYO7B	0.1046111	0.2222806	1.0873462	2.72E-06	1.68E-05
HPR	0.0597692	0.170914	1.5157953	0.0059913	0.0128278
ZNF683	0.735847	1.6212147	1.1395975	1.65E-08	2.24E-07
SERPINA5	0.2718396	0.6365837	1.2275947	1.29E-07	1.25E-06
CCL16	0.0181041	0.0608021	1.7478059	1.21E-05	6.06E-05
NPY4R2	0.0270375	0.0640713	1.2447186	3.27E-05	0.0001425
DLX6	3.7905803	1.6939424	-1.162034	3.86E-14	7.63E-12
BEST2	0.2045221	0.0644462	-1.666089	0.002366	0.0057471
OTOP3	2.5085762	0.7720377	-1.700126	4.79E-05	0.0001965
FLRT1	0.4106705	0.1719986	-1.255585	0.0004662	0.0014169
H2BFWT	0.4080163	0.1915233	-1.091107	1.09E-08	1.58E-07
KRT31	17.981514	6.6792187	-1.428763	8.55E-06	4.52E-05
MYBPHL	0.1148553	0.2664442	1.2140159	0.005567	0.0120261
FXYD2	0.1102049	0.4000492	1.8599896	0.0005839	0.0017207
FRRS1L	0.642227	0.316132	-1.022556	3.50E-08	4.19E-07
XAGE2	0.4809168	2.1562429	2.1646604	0.009531	0.0191264
CCDC198	0.0041808	0.0167982	2.0064615	0.0048026	0.0105733
FGF18	0.2855725	0.5761763	1.0126531	0.0004234	0.0013011
SLC7A3	0.3257648	0.0981679	-1.730507	0.00017	0.0005888
ANKRD63	0.1108615	0.0416234	-1.413291	1.90E-05	8.96E-05
KRT77	1.5890283	0.4779651	-1.733168	3.60E-09	6.34E-08
CD79B	2.2613714	5.1670529	1.1921437	7.07E-07	5.28E-06
ART3	0.1591688	0.653372	2.0373466	0.0262297	0.0459206
TMEM252	0.0214133	0.0475069	1.149627	0.0001131	0.000414
NUDT10	1.9866806	0.4079665	-2.283837	7.66E-18	6.95E-15
RND1	2.2876818	5.36803	1.2305063	4.64E-08	5.29E-07
ASB5	0.0070058	0.0168456	1.2657443	0.0047208	0.0104141
ANKRD34C	0.0561424	0.0152354	-1.881661	0.0187779	0.0344836
KCNK2	1.3335196	0.4568742	-1.54537	1.28E-08	1.81E-07
FAM129C	0.1330232	0.4440429	1.739021	0.0039297	0.0088979
DMRT1	0.4319931	0.1980641	-1.125041	9.92E-11	3.53E-09
PF4	0.1506186	0.3258198	1.1131746	0.0010635	0.0028753
CHRDL2	0.4443059	1.0335707	1.2180119	9.12E-06	4.77E-05
TRPM1	0.0761891	0.025589	-1.574062	3.13E-05	0.0001371
RASGRF1	0.3954077	0.8002272	1.0170686	2.55E-06	1.59E-05
CD5L	0.0261319	0.11149	2.0930281	0.0003525	0.0011088
TESC	2.2323846	5.4092	1.2768296	7.64E-06	4.10E-05
ATP13A5	1.8662652	0.7492507	-1.316634	3.14E-08	3.80E-07
SLC34A2	36.486695	76.949821	1.0765475	2.88E-05	0.0001275
CXCL11	3.4226313	8.2860173	1.2755729	1.64E-06	1.09E-05
KRT33A	2.6845056	0.4568862	-2.55475	1.21E-08	1.73E-07
C4BPA	9.0565855	20.094252	1.1497437	2.93E-05	0.0001298
THSD7B	0.7920998	0.3545512	-1.159688	6.89E-05	0.0002683
PDZK1IP1	21.66746	44.14561	1.0267399	6.08E-10	1.51E-08
LCN10	0.0118163	0.0334158	1.4997494	0.0001877	0.0006404
SLC18A1	0.0177969	0.1523422	3.0976189	3.81E-07	3.12E-06
ELAVL4	0.0670056	0.1690098	1.3347535	0.0065554	0.0138664
C4orf17	0.1201298	0.0432373	-1.474245	1.66E-05	7.97E-05
CCL1	0.0879403	0.1870005	1.0884456	0.0007686	0.0021697
MTMR7	0.2482749	0.4987849	1.0064793	0.0219968	0.0395018
IL21	0.0461726	0.0980564	1.0865745	5.32E-06	2.99E-05
B3GALT1	0.2184114	0.0920072	-1.247229	8.24E-05	0.0003135
TFAP2B	1.043221	0.3817787	-1.450236	0.0001044	0.0003858
STAR	2.4244287	1.0198979	-1.24922	5.50E-13	6.14E-11
TNNT3	2.5263328	1.1927067	-1.082805	0.0025647	0.0061599
GGTLC2	0.0235359	0.0471251	1.001632	0.0026424	0.0063248
MT1A	1.6563578	3.666412	1.1463546	1.91E-06	1.24E-05
GRK7	0.3018373	0.1473358	-1.034663	3.59E-13	4.47E-11
CDH12	0.558424	0.1354574	-2.043522	0.0001137	0.0004159
MMP28	2.7335907	5.7030779	1.0609435	1.09E-10	3.79E-09
SCML4	0.1341237	0.2741933	1.031629	1.88E-09	3.76E-08
BFSP2	0.1031266	0.2490305	1.2719053	4.31E-06	2.49E-05
LTB	6.251003	13.043109	1.0611282	1.26E-08	1.79E-07
OLR1	3.7624621	10.36381	1.4618056	4.45E-13	5.16E-11
MAGEA8	0.3620933	0.1235523	-1.55124	0.0129357	0.0249182
GGTLC1	0.3427286	1.0610344	1.6303327	6.11E-05	0.0002423
SBK3	0.0593398	0.136217	1.1988356	2.15E-12	1.70E-10
ALDH3B1	2.1487835	4.5422939	1.0799009	7.58E-14	1.24E-11
ATP4A	0.5479758	0.2011162	-1.446083	2.04E-08	2.65E-07
TMPRSS15	0.1229319	0.0439713	-1.483225	1.91E-09	3.79E-08
C4BPB	0.1403919	0.5391367	1.9411916	3.00E-09	5.44E-08
NTS	381.82766	135.42112	-1.495469	2.90E-10	8.27E-09
IHH	0.057204	0.3471409	2.6013328	2.80E-07	2.40E-06
CALN1	0.256728	0.1062806	-1.272362	0.0015697	0.00403
APOB	0.0234099	0.1490087	2.6702073	0.0137675	0.0263291
HNF4A	0.0508402	0.3188369	2.6487775	0.0005197	0.0015532
IL17A	0.0314198	0.0700971	1.1576829	0.0120472	0.0234379
ADAMTS16	0.5104217	1.0869073	1.0904672	5.54E-10	1.40E-08
CYP4F2	0.2060967	0.0731582	-1.494231	6.49E-05	0.0002547
TNFRSF17	1.9216319	4.1806295	1.1213881	4.35E-07	3.49E-06
CLIC5	0.6848823	1.631868	1.2525965	9.96E-09	1.47E-07
APOC4-APOC2	0.0506989	0.1145516	1.17597	0.0006462	0.0018735
MSLNL	0.1135002	0.3327715	1.551837	0.0188747	0.0346407
CLDN18	2.2949005	5.9519227	1.3749242	0.0019641	0.0049045
ACKR2	0.2356919	0.5242967	1.153481	0.0002446	0.0008065
HOXD13	5.0044547	2.2862803	-1.130211	7.19E-11	2.80E-09
SYT8	1.453108	3.5594524	1.2925133	0.0013807	0.0036109
APOH	0.1708589	0.6885246	2.0107027	1.88E-06	1.22E-05
LILRA4	0.3147137	0.6872806	1.1268593	4.65E-06	2.65E-05
CNTN6	0.0495673	0.1290335	1.3802839	3.76E-05	0.0001604
CBLN2	0.7364176	0.2682436	-1.45698	0.0267823	0.0467131
SLC24A4	0.0354133	0.0743503	1.0700452	6.32E-07	4.81E-06
UTS2	0.1186106	0.2412474	1.0242802	2.05E-05	9.59E-05
PLA2G2C	0.0096422	0.0242874	1.3327751	4.49E-06	2.57E-05
LRTM1	0.0559452	0.0238229	-1.231663	0.0024023	0.0058169
FGG	5.4690032	23.604324	2.1097014	0.0007656	0.0021632
1-Dec	0.3562467	0.1732357	-1.040141	0.002516	0.0060608
BAG4	15.723709	7.4400351	-1.07956	6.44E-17	4.52E-14
LPA	0.0816982	0.0400581	-1.028209	1.16E-06	8.03E-06
ZDHHC19	0.490635	0.2236457	-1.133435	0.0225966	0.0404228
KCNJ4	0.2056902	0.0662477	-1.634531	0.0012939	0.0034053
NUDT11	5.5662715	2.1272105	-1.387748	1.68E-23	8.65E-20
SLC1A7	0.1701901	0.3698014	1.1196034	3.93E-05	0.0001668
FCRL4	0.0853921	0.1712891	1.0042594	9.52E-07	6.80E-06
ASGR2	0.2312656	0.8942434	1.9511169	9.38E-08	9.54E-07
SLC51B	0.3127838	0.645199	1.0445787	1.42E-08	1.97E-07
PCED1B	2.8323011	5.706328	1.010588	2.98E-19	3.83E-16
CPA2	0.4345999	0.1954637	-1.152788	4.12E-08	4.81E-07
DUSP4	2.3018394	4.9718797	1.1110042	1.52E-13	2.17E-11
IGLL1	0.3130667	1.043949	1.7375093	3.94E-05	0.0001671
SLC22A31	2.6525876	5.4853287	1.0481777	2.95E-06	1.80E-05
KCNN4	3.2148269	8.9199645	1.4722969	1.87E-12	1.50E-10
TCEAL5	0.6856414	0.2749749	-1.318154	0.000258	0.000845
GMNC	1.3877074	0.1159096	-3.581632	0.0122671	0.0238117
UCP1	0.2140651	0.0711109	-1.589908	9.92E-08	1.00E-06
ALPP	0.0853205	1.2944923	3.9233502	4.54E-07	3.61E-06
SLC6A15	2.9196933	1.345702	-1.117458	2.87E-12	2.17E-10
FCRL5	0.867656	1.8493506	1.0918236	3.44E-07	2.86E-06
CNTFR	1.3760076	0.5940679	-1.211789	0.0010621	0.0028721
BEAN1	0.2118724	0.4307948	1.0238054	7.11E-08	7.56E-07
LRRC26	0.0506447	0.1277451	1.3347846	0.0006855	0.0019694

Table S1 (*continued*)

Table S1 (*continued*)

Gene	Group1mea	Group2mea	LogFC	P	FDR
PAK5	1.1828155	0.5448986	-1.118165	1.79E-11	9.34E-10
ST18	0.0463682	0.1444054	1.6389174	0.0009588	0.0026255
FAM71F1	0.4417845	0.1851149	-1.254922	1.85E-07	1.69E-06
PCARE	0.1611456	0.0783837	-1.039738	4.23E-06	2.45E-05
PCDH19	3.6455389	1.8208415	-1.001527	3.68E-11	1.65E-09
ARRDC5	0.1114606	0.2313385	1.053472	1.56E-12	1.35E-10
SELENOV	0.1470971	0.056689	-1.375629	1.42E-05	6.96E-05
GJB1	0.4665419	1.7810383	1.9326399	0.0002844	0.0009187
PADI4	0.0846064	0.1696696	1.0038884	0.0002209	0.0007391
IGSF23	0.0378297	0.1024343	1.4371073	0.0054235	0.0117405
PDK4	2.1267715	4.6818061	1.1384002	2.26E-08	2.90E-07
SP8	0.8266877	0.3700295	-1.159702	2.00E-06	1.29E-05
RBFOX1	0.0730287	0.0208249	-1.810152	0.0001165	0.0004245
CD40LG	0.3169559	0.7401606	1.2235563	1.69E-09	3.43E-08
KCNJ18	0.0437124	0.1616592	1.8868398	0.0256232	0.0450327
AGER	8.5470901	24.774319	1.5353402	0.0001049	0.0003874
CFB	1.6329372	3.5973609	1.1394696	1.08E-12	1.04E-10
C1orf127	0.0765173	0.3589148	2.2297843	1.04E-07	1.05E-06
ACKR1	2.9808929	6.3184116	1.0838174	0.0001379	0.0004915
KIR2DL1	0.0346122	0.0705239	1.02683	2.99E-05	0.0001317
RIIAD1	0.0538496	0.1159582	1.1065989	0.0196227	0.0358132
CYP1A2	0.0485942	0.0993048	1.0310796	0.0013468	0.0035316
FCER2	0.2466865	0.9269581	1.9098256	0.0020106	0.0050053
MEP1A	0.0704701	0.1819437	1.3684078	0.0011311	0.0030299
CD19	1.1214511	2.6630966	1.247738	0.0001441	0.0005107
SAA2	2.2668547	5.3495566	1.2387274	1.72E-06	1.14E-05
KRT85	0.4674078	0.0369487	-3.661088	7.71E-06	4.13E-05
NR1H4	0.0155795	0.0583645	1.90544	0.0003515	0.0011062
EXOC3L4	0.5735585	1.1850551	1.0469415	3.29E-05	0.0001431
PNOC	0.6506501	1.4522507	1.1583367	3.10E-05	0.0001359
ACSL5	4.4796977	9.5259197	1.088457	8.64E-14	1.40E-11
TNFRSF13B	0.1799647	0.4367933	1.2792368	1.37E-05	6.74E-05
CST6	4.2451032	11.931948	1.4909581	2.68E-09	4.94E-08
CCDC177	0.4474395	0.1887677	-1.245081	8.46E-07	6.13E-06
CPM	3.8658728	19.177713	2.3105646	4.33E-11	1.87E-09
NLRP12	0.0655483	0.1382745	1.076904	1.91E-09	3.79E-08
DLX2	0.861191	0.3909224	-1.139451	9.24E-08	9.43E-07
KRT71	0.0887235	0.0357059	-1.313155	1.91E-07	1.74E-06
PRKG2	1.4162709	0.6488038	-1.126243	4.80E-15	1.61E-12
NR5A1	0.9553492	0.2046152	-2.223115	3.14E-05	0.0001371
JCHAIN	162.39442	326.81161	1.0089571	1.04E-06	7.30E-06
TH	0.157002	0.4503593	1.5202938	0.010532	0.0208665
DDN	0.6593063	0.313915	-1.070575	5.49E-11	2.26E-09
CST5	0.0857647	0.2195112	1.3558384	0.0028918	0.0068421
PLEKHB1	1.6364164	3.2958772	1.0101226	0.001647	0.004197
ATP2A3	4.2175949	8.8189994	1.0641945	3.79E-10	1.02E-08
PRSS41	0.3187017	0.1204352	-1.403949	0.0150291	0.0284321
NPY	5.2893793	0.2325927	-4.507221	0.0140235	0.0267529
CPB1	0.0404718	0.2451016	2.5983921	0.0095104	0.0190901
NGB	0.8988258	0.4335388	-1.05188	0.0234196	0.0417111
GALNT8	0.2621185	0.1222182	-1.10076	2.41E-05	0.0001098
UGT2A1	1.5754727	0.3526817	-2.159346	9.45E-06	4.90E-05
EMX2	0.2712342	0.1074359	-1.336063	0.0012851	0.0033843
AL035425.2	0.6626827	0.0899352	-2.88136	6.16E-08	6.71E-07
GAST	4.5618549	2.0507868	-1.153443	6.86E-08	7.31E-07
SMOC1	1.8019301	3.6952424	1.0361259	0.0024847	0.0059929
ATP1A2	0.1105655	0.2663837	1.2686042	0.001139	0.0030473
DMRT2	7.8776831	3.8360008	-1.038168	3.74E-09	6.55E-08
FOXI3	2.0647373	0.9238774	-1.160185	2.65E-05	0.0001192
MARCO	8.6583528	18.10752	1.0644245	4.34E-05	0.0001808
DUSP1	56.090465	115.30344	1.0396081	1.87E-14	4.65E-12
TMPRSS3	0.6275687	1.6836183	1.4237199	4.18E-10	1.10E-08
KCNH5	0.0743964	0.0291946	-1.349532	2.58E-07	2.24E-06
CA5A	0.0075099	0.0568675	2.9207466	0.0115052	0.0225027
LIPK	0.2279685	0.6214805	1.4468748	0.0057435	0.0123554
NCAN	0.044714	0.0218467	-1.033311	0.0017052	0.0043299
CTLA4	1.2499814	2.5059655	1.00346	4.37E-10	1.14E-08
GPR15	0.7753554	1.9007656	1.2936509	0.0001076	0.0003964
LRRN4	0.4714254	1.0147338	1.1059999	0.0002196	0.0007351
SLC5A7	0.857983	0.4108172	-1.062453	3.32E-05	0.0001441
CD300LG	0.0362632	0.1143204	1.656505	0.0022825	0.0055822
OR4C6	0.018105	0.0579231	1.6777512	4.05E-06	2.36E-05
CHI3L2	1.5916937	4.34548	1.4489528	1.36E-08	1.90E-07
RRAD	4.6072052	10.882975	1.2401093	1.75E-07	1.62E-06
C15orf53	0.019083	0.0403618	1.0807054	5.02E-08	5.67E-07
OR6C70	0.2710429	0.1181325	-1.198115	2.67E-06	1.65E-05
CNGA3	0.0182579	0.0522951	1.5181554	0.0228602	0.0408251
ENTPD8	0.3253159	0.7643812	1.2324509	0.0006042	0.0017688
POU5F1B	0.4212823	0.160381	-1.393284	2.52E-08	3.16E-07
BTN1A1	0.061885	0.2270137	1.8751183	0.0004588	0.0013974
KRT7	30.032808	76.150743	1.3423187	8.56E-08	8.85E-07
FGL1	0.0640789	1.4708639	4.5206697	0.0009194	0.0025315
TMEM211	0.3389852	0.1373935	-1.302908	0.0003985	0.001235
SOAT2	0.0445686	0.1378471	1.6289703	3.95E-05	0.0001672
ART4	0.0715704	0.3228416	2.1733916	2.19E-07	1.95E-06
CYP8B1	0.0176483	0.0504627	1.5156897	1.27E-07	1.24E-06
DCSTAMP	0.3132697	0.6466832	1.0456539	3.09E-05	0.0001353
ZNF556	0.5340905	0.2264063	-1.23817	2.28E-09	4.33E-08
DNASE2B	0.203546	0.4108932	1.0134089	0.0083295	0.01703
SERPINA4	0.0708358	0.2457923	1.7948887	0.0004813	0.0014555
KLHDC7A	0.2855438	0.5885613	1.0434807	1.11E-05	5.64E-05
MAGEA9	0.5715574	0.238541	-1.260661	4.21E-06	2.44E-05
HLA-DRB5	72.820433	147.03934	1.0137869	7.78E-10	1.86E-08
CACNG5	0.0879349	0.0332525	-1.402971	0.0147258	0.0279166
PRR26	0.0402988	0.0850317	1.0772638	5.53E-05	0.0002222
GABBR2	0.1583002	0.3594661	1.1831926	0.0017622	0.0044548
CNR2	0.0845694	0.2158409	1.35176	0.0006858	0.0019695
S100Z	0.0546434	0.1144125	1.0661258	3.54E-11	1.59E-09
LY6H	0.392329	0.8033406	1.0339477	3.75E-05	0.0001602
VEPH1	0.4303532	0.8693296	1.0143821	0.0011651	0.0031059
HGD	0.4184698	3.165996	2.9194641	8.82E-06	4.65E-05
PRG4	0.3022066	0.6807574	1.1716055	3.60E-05	0.0001549
CCL15	0.0359465	0.1480815	2.0424671	2.21E-05	0.0001024
ELANE	0.0570853	0.1152135	1.0131195	8.08E-10	1.91E-08
C9orf152	0.6823415	1.4740895	1.1112583	3.14E-05	0.0001371
TIMD4	0.2352412	0.5331891	1.1805062	7.67E-05	0.0002946
KCNH6	0.0326766	0.4111455	3.6533195	0.017391	0.0323449
TFPI2	3.8848397	17.652384	2.1839361	4.34E-07	3.48E-06
NR2E1	0.2424586	0.1023293	-1.244519	0.0002337	0.000775
UGT1A8	1.190514	0.436199	-1.448526	0.0001053	0.0003886
COL4A4	0.6408318	1.3279507	1.051184	2.40E-08	3.04E-07
C7	5.6482	11.844127	1.0683088	2.45E-05	0.0001114
PCDHA12	0.0475304	0.1091049	1.1987922	1.24E-05	6.20E-05
NAPSA	27.395519	57.651458	1.0734172	0.0001306	0.0004692
ZNF80	0.0569966	0.1255091	1.138844	1.75E-10	5.60E-09
RTP5	0.0381554	0.0815663	1.0960865	3.22E-06	1.94E-05
PRAC2	1.2864859	0.4011501	-1.681222	6.59E-07	4.97E-06
PAEP	1.9192878	4.7342152	1.3025542	9.53E-05	0.0003564
SPDEF	1.4355079	4.9460727	1.7847222	4.10E-07	3.32E-06
DMRT3	2.1029536	0.991216	-1.085146	2.24E-09	4.26E-08
AZGP1	5.466691	15.116574	1.4673914	0.0095097	0.0190901
CALHM4	0.055558	0.0248775	-1.159149	0.0074787	0.0155524
SIX3	1.1355632	0.5539238	-1.035649	5.77E-05	0.0002304
C16orf54	1.1613435	2.3257427	1.0018968	3.66E-10	9.91E-09
KRT37	0.2245018	0.1040464	-1.109499	0.0047109	0.0103972
IRS4	2.2113177	0.3073318	-2.847037	3.79E-15	1.36E-12
RP1	0.0204568	0.074226	1.859345	0.0006661	0.0019216
SERPINA9	0.0917988	0.2864549	1.6417614	0.0015375	0.0039598
COLEC10	0.6814836	0.2908355	-1.228475	6.76E-06	3.69E-05
C9orf135	0.2671979	0.6476836	1.2773805	0.0258438	0.0453582
ARL14EPL	0.0163073	0.0449301	1.4621609	1.72E-05	8.23E-05
CIITA	1.5173457	3.0540657	1.0091813	1.44E-12	1.29E-10
MUC5B	2.0503223	4.8456646	1.2408438	0.0244833	0.0432857
TCL1A	0.5331663	1.6654578	1.6432611	0.0275439	0.0477982
ZFP57	0.3003402	0.818163	1.4457909	0.001198	0.0031838
ZNF831	0.1462374	0.3206646	1.1327526	9.03E-09	1.35E-07
PTGDS	13.040409	28.56222	1.131119	2.18E-07	1.95E-06
MYOCD	0.0537043	0.1184346	1.14098	0.0002947	0.000947
SULT1E1	3.7743628	1.8362406	-1.039478	0.0246026	0.043472
DPEP1	0.5731002	1.3211239	1.2049063	1.44E-06	9.71E-06
FOXA2	0.8956215	2.4305829	1.4403413	2.83E-05	0.000126
HBE1	1.1797805	0.4148783	-1.507758	0.0064335	0.0136475
LMO3	0.9826354	2.1650636	1.1396813	0.0001825	0.0006254
RGS13	0.1028473	0.2524533	1.2955121	1.79E-05	8.55E-05
SLC6A14	4.1671447	9.5148351	1.1911195	0.0001189	0.0004319
KRT38	0.2955612	0.0933271	-1.663089	8.08E-05	0.0003079
FAM43B	0.2295253	0.5057907	1.1398874	0.0050513	0.0110404
NPY5R	0.0360308	0.0160795	-1.164004	0.0220132	0.0395213
DLX5	17.520582	7.2836436	-1.266318	1.39E-11	7.62E-10
MYH6	0.0399018	0.0168768	-1.241412	0.0002211	0.0007394
FCRL3	0.3173762	0.6892636	1.118862	9.36E-06	4.86E-05
MOGAT2	0.0706173	0.1761504	1.3187144	0.001461	0.0037905
AGRP	0.1539972	0.3143312	1.029381	3.51E-05	0.0001513
SFTA2	8.652021	20.374667	1.2356674	2.22E-05	0.0001025
FCAMR	0.074069	0.229677	1.6326657	0.016766	0.031326
DPYSL5	0.6195981	0.2617078	-1.243376	0.00728	0.0152022
PRSS50	1.7524226	0.8377435	-1.06477	0.0240373	0.042623
FAM135B	0.0058464	0.0179051	1.6147458	0.0005847	0.0017225
RTP1	0.2080361	0.0552048	-1.913968	0.0002678	0.0008718
MPP4	0.1993077	0.0624942	-1.673203	5.55E-10	1.40E-08
C5AR2	0.3392783	0.6979786	1.0407135	1.06E-14	3.04E-12
CTCFL	1.7241705	0.5806367	-1.570195	0.0001625	0.000566
SFTA3	1.6029251	4.7017735	1.5524981	6.14E-06	3.40E-05
ADRA2B	2.8502782	0.734125	-1.957005	2.85E-14	6.29E-12
KRT86	1.0146951	3.9761122	1.9703121	0.0171615	0.0319758
FCRLA	0.9141016	1.8765963	1.0376919	7.85E-06	4.20E-05
GAS2L2	0.1858245	0.3876721	1.0608964	0.0066459	0.0140306
TMSB15A	5.9195085	2.6037178	-1.184904	2.43E-05	0.0001108
CYP27B1	1.6872306	4.1805553	1.3090374	0.0025405	0.0061064
SLC9A4	1.1141609	0.3363362	-1.727982	3.40E-09	6.04E-08
FCRL1	0.1893282	0.6398689	1.7568868	6.05E-05	0.0002402
CDSN	0.0859451	0.1743006	1.0200905	0.0216537	0.038962
NCR3LG1	0.9710002	0.4191052	-1.212159	1.30E-12	1.20E-10
TLX1	1.0847874	0.5322425	-1.027257	4.73E-05	0.0001944
PAX2	0.1407418	0.0582337	-1.273126	0.0122307	0.0237529
POU3F3	0.3105651	0.0391406	-2.988156	0.0001523	0.0005347
CAMP	0.3836411	0.8933575	1.2194803	0.0132592	0.0254497
LCNL1	0.0805885	0.1690874	1.0691227	0.0001565	0.0005483
R3HDML	0.0912046	0.2341488	1.3602465	0.0001572	0.0005502
RORC	0.663265	1.5914862	1.2627173	6.18E-10	1.52E-08
FEZF1	2.9286284	1.0543795	-1.473831	8.39E-17	5.63E-14
IGFALS	0.1656319	0.3572974	1.1091454	3.65E-05	0.0001566
ASTN1	0.290696	0.1158457	-1.327306	0.0001542	0.0005406
PROKR1	0.0709272	0.0330461	-1.101861	3.45E-05	0.0001494
AL645922.1	0.0026926	0.005609	1.0587678	2.46E-06	1.54E-05
SOD3	5.6097691	12.042181	1.1020834	5.90E-13	6.50E-11
CYP24A1	6.1546606	14.771442	1.2630595	1.28E-05	6.35E-05
NUTM1	0.1315199	0.0245614	-2.420815	1.09E-05	5.56E-05
PLA2G12B	0.1804287	0.6559999	1.8622669	0.0144967	0.0275365
RASGRP2	0.6199086	1.39513	1.1702722	1.40E-07	1.35E-06
MS4A3	0.0105045	0.0230713	1.1350922	0.0197903	0.0360593
DNAJC12	0.8844665	2.889493	1.7079369	0.0146015	0.0277082
CCBE1	0.4205653	0.8666158	1.0430625	9.96E-06	5.13E-05
TMEM271	0.2110363	0.0546818	-1.948358	2.17E-08	2.79E-07
ANKRD1	0.5690641	1.5274807	1.4244911	2.67E-07	2.31E-06
FOLR1	5.8530584	13.166446	1.1696034	6.80E-06	3.71E-05
SYT2	0.5531923	0.272185	-1.023193	0.0014211	0.0037058
TDRD12	1.65162	0.4574519	-1.85219	0.0211226	0.038149
OTOP2	0.2685855	0.1238648	-1.116615	1.18E-08	1.70E-07
UNC5A	0.1392451	0.2940989	1.0786752	4.14E-08	4.82E-07
OR51B5	0.1836951	0.0825315	-1.154295	0.0013966	0.0036476
HSF5	0.015598	0.0320273	1.0379462	0.0001052	0.0003884
TCF21	0.3733349	0.7928844	1.0866403	7.06E-09	1.11E-07
LHX8	0.3903333	0.1378984	-1.501101	0.0002761	0.0008954
C10orf90	0.1574476	0.0672942	-1.226317	0.0007653	0.0021628
IL17C	0.0969237	0.2243141	1.2105992	0.0005819	0.0017159
ATOH8	0.5387376	1.2639946	1.2303356	7.56E-09	1.17E-07
NKX2-1	2.4965351	8.2009172	1.7158581	3.68E-06	2.18E-05
KCNK3	0.6774485	1.4452751	1.0931609	7.72E-06	4.14E-05
OPRD1	0.0440164	0.112539	1.3543105	0.0152077	0.0287278
CXCR5	0.0428159	0.0988855	1.2076112	1.48E-05	7.21E-05
CYP2W1	2.533619	1.0689299	-1.245032	1.05E-05	5.38E-05
RGS7	0.0291337	0.1203007	2.0458865	0.0162217	0.030427
AICDA	0.0493865	0.153574	1.6367452	0.0008697	0.0024159
AKAP2	0.0406772	0.0866811	1.0914951	3.60E-10	9.87E-09
PLA2G1B	0.6183673	1.3054453	1.0780062	0.0002352	0.0007792
CRHR2	0.3535215	0.1717883	-1.041166	0.000549	0.0016307
FOXH1	0.4508891	0.1448941	-1.637774	2.26E-07	2.01E-06
TNR	0.0317226	0.0681065	1.1022806	0.0046547	0.0102872
UGT2B4	0.0337059	0.1493951	2.1480579	0.0049916	0.0109301
ADRA1B	0.224057	0.5474622	1.2888935	2.09E-07	1.88E-06
C8A	0.0117988	0.0658031	2.4795154	4.45E-06	2.55E-05
HLA-DQA2	14.686225	30.391381	1.0491986	4.38E-06	2.52E-05
COL4A3	0.3174126	0.7671973	1.2732384	2.51E-09	4.67E-08
AC119396.1	0.1692677	0.3463526	1.0329349	7.33E-07	5.44E-06
SP5	0.744994	1.5035463	1.0130686	0.0049361	0.0108285
CHIA	0.1356457	0.2732265	1.0102544	0.0002592	0.0008486
NRXN1	0.4069005	0.1728911	-1.234813	4.98E-07	3.92E-06
C11orf87	0.4943109	0.1801545	-1.456184	7.05E-06	3.83E-05
TMEM132D	0.0507897	0.1060506	1.0621458	0.000478	0.0014473
FGA	1.5061924	10.204672	2.7602519	0.0020456	0.0050848
TGM2	19.968072	44.693075	1.1623563	3.34E-14	6.97E-12
AC008878.3	0.0050541	0.0128422	1.3453658	7.30E-06	3.95E-05
NDNF	2.6800456	5.6954556	1.0875537	0.0004152	0.001279
NYAP2	0.0414728	0.0925343	1.1578249	0.0002259	0.0007531
SUSD2	3.5275558	7.976981	1.1771739	2.93E-06	1.78E-05
TNNC1	1.2291344	2.6287371	1.0967272	5.69E-05	0.0002278
DNALI1	1.0946023	2.6967863	1.3008345	0.0006172	0.0018027
AP000781.2	0.0389015	0.0849121	1.1261455	2.30E-09	4.35E-08
FAM107A	0.8889839	2.0600664	1.2124617	0.0001094	0.000402
CRIP1	0.8207881	1.7176597	1.0653626	1.15E-14	3.16E-12
GPC3	80.629963	33.4392	-1.269776	8.38E-11	3.16E-09
CCDC190	4.2454206	1.9810781	-1.099622	1.21E-07	1.18E-06
SUCNR1	0.9228962	1.8793326	1.0259801	9.66E-05	0.0003607
ADAMTS8	0.2953829	0.6198415	1.0693133	0.0022677	0.0055548
TMEM100	0.9559432	1.9551469	1.0322802	0.0004285	0.0013143
ADH1B	1.4030209	3.1596085	1.1712093	0.0024018	0.0058167
PTPRT	1.0284778	0.4234125	-1.280375	0.000143	0.0005077